The Meteoritical Society

Meteoritics & Planetary Science 43, Nr 9, 1497–1516 (2008)
Abstract available online at http://meteoritics.org

Correlated isotopic and microstructural studies of turbostratic presolar graphites from the Murchison meteorite

Thomas K. CROAT*, Frank J. STADERMANN, and Thomas J. BERNATOWICZ

Department of Physics and Laboratory for Space Sciences, Washington University, Campus Box 1105, One Brookings Drive, Saint Louis, Missouri 63130–4862, USA
*Corresponding author. E-mail: tkc@wustl.edu

(Received 26 December 2007; revision accepted 29 March 2008)

Abstract–We present data from TEM and NanoSIMS investigations of Murchison (CM2) KFC1 presolar graphites. TEM examinations of graphite ultramicrotome sections reveal varying degrees of graphite disorder, leading to distinctions between well-graphitized onions, more turbostratic platy graphites, and the most disordered cauliflower graphites. Aside from their larger size, platy graphites are roughly similar in isotopic composition and in internal grain properties to the well-graphitized onions. Most carbide-containing platy graphites exhibit large s-process element enrichments (~200× solar Mo/Ti ratios), suggesting origins predominantly in AGB carbon stars. The C isotopic distribution of platy graphites is similar to onions, with representatives in both ^{12}C-depleted ($5 < {}^{12}C/{}^{13}C < 40$) and ^{12}C-enriched groups ($100 < {}^{12}C/{}^{13}C < 350$) and a pronounced gap in the $40 < {}^{12}C/{}^{13}C < 75$ region that contains 75% of mainstream SiCs. The large ^{12}C enrichments combined with the extreme s-process element enrichments suggest formation in an environment inhomogeneously enriched in the nucleosynthetic products of thermal pulses in AGB stars. In contrast, numerous scaly cauliflower graphites show ^{18}O enrichments and lack s-process-enriched carbides, suggesting a SN origin, as was the case for many Murchison KE3 SN graphites. The more turbostratic graphites (platy and scaly) are on average larger than onions, likely resulting from formation in a gas with higher C number density. Oxygen content increases progressively with increasing degree of graphite disorder, which can stabilize these grains against further graphitization and may be a reflection of higher O/C ratios in their formation environments.

INTRODUCTION

Presolar grains of stardust, found preserved within primitive meteorites and IDPs, are samples produced by ancient stars that contain clues into their inner workings as well as detailed information about the population of stars that contributed material to the solar system. Most presolar grains that condensed in the outflows of asymptotic giant branch (AGB) stars or supernova (SN) explosions are ~1 μm or smaller, and only recently have sufficiently high resolution microanalytical instruments (such as NanoSIMS) become available to study the isotopic compositions of these submicron materials in detail (Clayton and Nittler 2004). Coordinated transmission electron microscopy (TEM) and NanoSIMS investigations of presolar grains have begun to reveal rich and diverse information (Messenger et al. 2005; Nguyen et al. 2007), especially for graphites that contain populations of presolar grains trapped within presolar grains (Croat et al. 2005; Stadermann et al. 2005). These graphite "time capsules" are quite effective at capturing and preserving grains of higher temperature condensates that formed prior to graphite (in one case more than a thousand 30 nm-sized internal carbides were present within a single 6 μm-sized graphite; Croat et al. 2003). The list of higher-temperature minerals discovered as internal constituents of presolar graphites has grown quite long, including refractory Ti, Zr, Mo, Ru, Fe carbides, silicon carbide, metallic Al, FeNi, Ru, and Os, along with various oxide phases (rutile, chromite, eskolaite, etc.; Bernatowicz et al. 2006). These assemblages of different phases can be used to infer the phase condensation sequence, which along with equilibrium condensation calculations, can provide detailed information about the pressures, temperatures, and C/O ratios during grain formation (Bernatowicz et al. 1996, 2005, 2006).

Previous isotopic studies of Murchison KFC1 residues (Amari et al. 1994) have shown that only graphite spherules are presolar, whereas the aggregates and non-round compact carbonaceous grains that are also present lack C anomalies

(Hoppe et al. 1995; Zinner et al. 1995). Further distinctions among the round grains were made between "onion" and "cauliflower" graphites based on the surface morphology in scanning electron microscopy (SEM), and these surface structures reveal a variable degree of graphitization. Along with the morphological differences, onions on average tend to be isotopically lighter and had lower trace element content, whereas cauliflowers show a wide range of C anomalies and sometimes higher trace element content. TEM imaging and diffraction studies of ultramicrotomed graphite slices (Bernatowicz et al. 1991, 1996) reveal the structural differences, in regularity and long-range continuity of the stacking of graphene sheets, that lead to the different external morphologies of onions and cauliflowers. The smooth, outer shells of the onions are formed by well-crystallized graphitic layers, although in many cases the grain cores are nanocrystalline. In contrast, cauliflowers are composed of short, curved and discontinuous (turbostratic) layers. Previous TEM studies (Bernatowicz et al. 1996; Croat et al. 2005) have focused almost exclusively on the more abundant onions, although two cauliflower graphites were studied from an earlier Murchison LFC1 separate (Bernatowicz et al. 1991). However, due to instrumental limitations and the small size of the KFC1 onion graphites, correlated isotopic and TEM studies on the exact same spherules have only been done recently.

In the Croat et al. (2005) study of Murchison KFC1 onions, the ability to correlate TEM and isotopic measurements led to unique insights into their formation environment. Most (85%) of the internal carbides within onion graphites were heavily enriched in s-process elements (Zr, Mo, and Ru), with a median enrichment of ~200× solar. Many of these same carbide-containing graphites showed isotopically light carbon (mostly in $100 < {}^{12}C/{}^{13}C < 400$ range). Although an AGB carbon star origin is suggested by the s-process enrichment, both the s-process element and ^{12}C enrichments considerably exceed that astronomically observed around carbon stars (Croat et al. 2005; Lambert et al. 1986). However, both ^{12}C and s-process elements are formed in great quantities during thermal pulses, and their observation together suggests that these graphites may have formed in chemically and isotopically inhomogeneous regions around AGB stars, such as high density knots or jets. Detailed considerations of graphite growth in AGB outflows (Bernatowicz et al. 2005, 2006) led to the conclusion that the gas densities must also be inhomogeneous, and must exceed those expected from smooth mass outflows to allow formation of micron-sized graphites.

In this work, we will investigate the chemical and isotopic properties of round turbostratic graphites (both "platy" and "scaly" morphologies as defined below), and then compare these results to both the morphologically similar Murchison KE3 SN graphites (Croat et al. 2003) as well as to the well-graphitized Murchison KFC1 onions (Croat et al. 2005). All of the more turbostratic graphites are larger on average than onions. The scaly morphology is most similar to the "cauliflower" graphite group, whereas many of the platy graphites were likely lumped in with onions in previous SEM-SIMS studies (Hoppe et al. 1995; Zinner et al. 1995). The morphological differences between the onion and cauliflower types probably reveal differences in formation conditions, rather than being ascribed to later processing or heating (e.g., Bernatowicz et al. 1996). For example, changes in the rapidity of formation or in the circumstellar chemical environment (e.g., C/O ratio in the gas) could alter their degree of graphitization. We seek to find any correlations between the morphological types and the likely stellar sources (e.g., supernovae, AGB carbon stars, etc.) as well as to look for any clues into the nature of the different degrees of graphitization seen among presolar graphites. In addition, we investigate the properties of internal grains of other phases within the graphites, such as the degree of s-process enrichment in refractory carbides that indicates an AGB carbon star origin. We have the advantage of working with many hundreds of presolar graphites sliced en-masse, each of which allows a unique observation of an ancient (now extinct) star. Through detailed studies of this population of grains, we hope to refine our knowledge of the population of stars that contributed material to our solar system.

EXPERIMENTAL PROCEDURES

Through the procedures of Amari et al. (1994), presolar graphites from the Murchison meteorite have been concentrated in the KFC1 density and size separate (2.15–2.20 g cm^{-3}; >1 μm). The resulting KFC1 graphite population has been characterized previously using SEM surface morphology and SIMS analyses (Hoppe et al. 1995; Zinner et al. 1995). Approximately 95% of these graphites show carbon isotopic anomalies, ranging from $2 < {}^{12}C/{}^{13}C < 7300$ (0.02 to 80 times the solar value of 89). For TEM studies, KFC1 graphites were deposited from suspension, embedded in resin, sliced into <100 nm thick ultramicrotome sections, and retrieved on carbon-coated copper TEM grids (further details in Bernatowicz et al. 1996). The exact number of graphites originally deposited from suspension is unknown, but at least ~300 unique graphites are present, as this many have been observed in a single ultramicrotome slice. Although only 5–10% of the graphite volume is available for subsequent analysis, this slicing method allows us to quickly study a significant fraction of the KFC1 population. To individually pick, mount in resin, ultramicrotome and examine this number of graphites using the same method as was used for KE3 SN graphites (Croat et al. 2003) would entail several decades of work.

Cross-sections of graphites were studied using a JEOL 2000FX TEM equipped with a NORAN ultra-thin window energy dispersive X-ray spectrometer (EDXS) and a Gatan

model 666 electron energy loss spectrometer (EELS). Approximately ~1500 graphite sections were studied overall from ~23 unique microtome slices. It is virtually certain that multiple sections have been studied for some graphite spherules, but correlating these observations is quite difficult given the technique used. Selected-area diffraction (SAD) patterns and bright and dark field images were used to better characterize the structural differences between the graphite types. Dark field images (created from the electrons diffracted by the {002} crystal planes rather than the direct electron beam) were used to determine the size of ordered structural domains, which aided in classifying graphites.

Both onion-type and cauliflower-type KFC1 graphites often captured and preserved other higher-temperature stellar condensates during their growth, and these internal grains give further important clues about grain condensation in stellar outflows. Therefore, graphites were searched for internal grains by observation at high magnifications (~10^5) during tilting of the specimen stage, and grains as small as 5 nm became clearly visible when in an orientation satisfying the Bragg diffraction condition (further details in Croat et al. 2003). At this lower size limit, some graphite types showed many coherently scattering graphitic domains in bright field images which could mask the presence of internal grains. However, even in such cases any internal grains could be distinguished based on EDXS.

Quantitative EDXS analysis was performed on all internal grains using k-factors derived from geological standards of known composition (ilmenite USNM 96189, chromite USNM 117075, basaltic glass USNM 113498) and numerous stoichiometric oxides (lead titanate, lead zirconate, lead molybdate, calcium vanadate, calcium titanate, calcium phosphate, etc.) using the Cliff-Lorimer technique. Derived k-factors for elements with Z > 11 with respect to Ti (directly or indirectly) typically showed 3–10% variations (std. dev.). Further details on the methods employed are available in Croat et al. (2005). EDXS spectra were also collected from background regions in the graphite (free of internal grains), and these showed C and O with occasional Ca, Cr, and Fe peaks along with other background peaks (Cu from grid, Si contribution from intrinsic detector peak). Due to various difficulties such as the absorption of light element peaks, standardless analysis was used for oxygen. Thus the oxygen content of graphites (O/C count ratio) is only used as a comparative measure between the various morphological types. These graphite spectra were generally collected from regions with holes in the embedding resin and also holes in the carbon grid where possible, minimizing any possible contributions from the resin or the carbon coating on the copper grid. EELS spectra from ~200–700 eV (encompassing the 284 eV C-K and 532 eV O-K peaks) were also collected to compare the oxygen content. Power-law background fits were first subtracted and then 50 eV width integrations (at 40–50 eV above C-K and O-K edges) were used. Good agreement between relative oxygen content as measured by EELS and EDXS was obtained, although the excessive EELS background in onion graphites and contributions from the background grid were problematic.

The crystal structures of many internal grains were determined with selected area diffraction (SAD) and/or microdiffraction. Grains showing EDXS compositions consistent with common refractory carbides were typically identified on the basis of a single low-index zone axis pattern, whereas 3–4 major zones were typically acquired for other grains with abnormal compositions. The diffraction rings from {100} and {110} graphite served as an internal calibration for d-spacings (~1% accuracy) as well as for astigmatism correction.

After TEM analyses, the TEM grid was mounted in a conducting, clamping holder and analyzed in the Cameca NanoSIMS (SIMS = secondary ion mass spectrometry). A ~100 nm diameter Cs^+ primary beam was rastered over the graphites and secondary electrons and negative secondary ions ($^{12}C^-$, $^{13}C^-$, $^{16}O^-$, $^{18}O^-$ and either $^{17}O^-$ or $^{28}Si^-$) were simultaneously collected. The carbon film also present in the NanoSIMS isotopic images was used as a standard to calibrate C and O isotopic ratios. Measurement time was usually limited by sputtering deterioration and failure of the underlying grid, although in most cases more graphite material remained after C and O measurements. Further experimental details can be found in Stadermann et al. (2005).

RESULTS

Morphology and Microtexture of Graphite Spherules

Presolar graphite spherules from Murchison were first classified as different "vegetable" types based on their surface morphology, and Fig. 1 shows representative SEM images of an onion and a cauliflower graphite. Further insights into these structures came from subsequent TEM investigations of ultramicrotomed graphites, wherein onions with and without cores, platy turbostratic graphites, and scaly cauliflower graphites were found (Fig. 2). Onions with and without nanocrystalline carbon cores (Fig. 2a) comprise a majority of presolar graphites (about ¾ of population by number), and their properties have been previously discussed at length (Bernatowicz et al. 1996; Croat et al. 2005). Among the more turbostratic graphites, Bernatowicz et al. (1991) made the distinction between platy graphites (Fig. 2b) with continuous concentric layering and well developed (002) lattice fringes and scaly cauliflower graphites (Fig. 2c) with short, curved and discontinuous layers that lack long range continuity. In terms of appearance, both these turbostratic graphite types are more similar to platy-like, lower-density KE3 graphites of SN origin than to the well-graphitized onions. As with the onions, a subset of the platy graphites had nanocrystalline cores

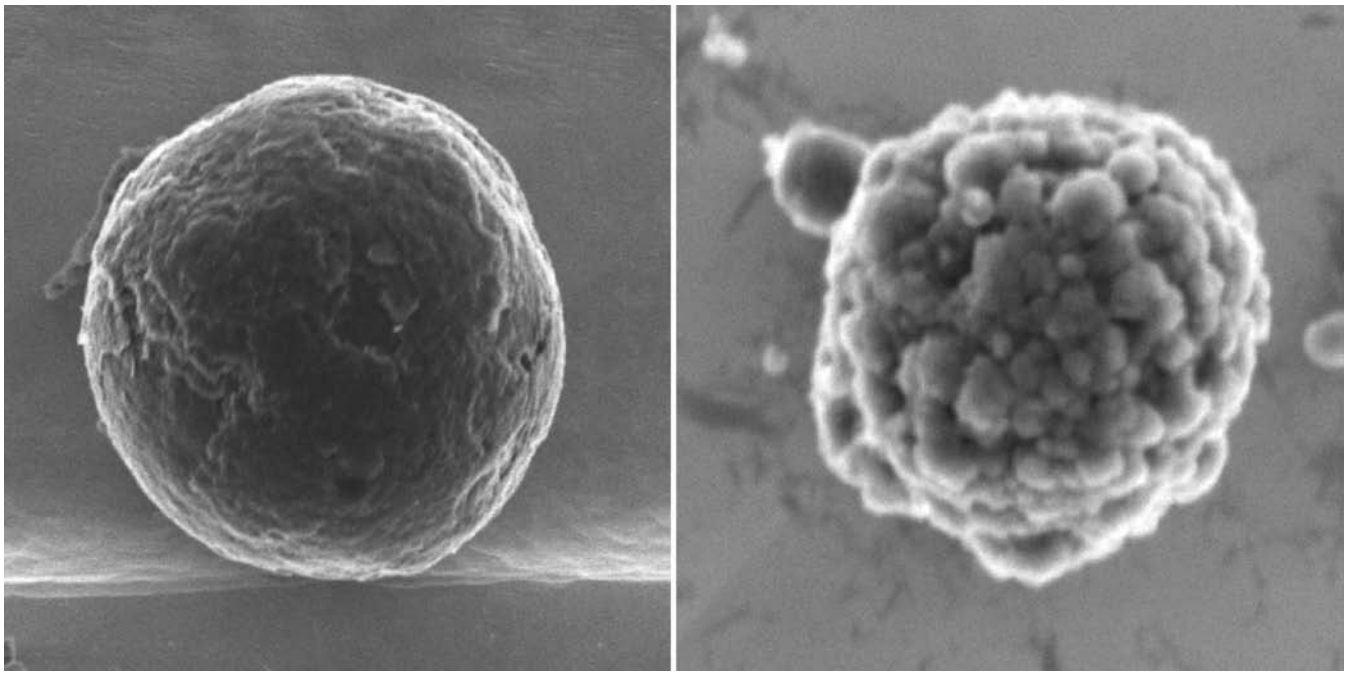

Fig. 1. Representative SEM images of Murchison onion and cauliflower graphites.

(~30%), with similar diffraction patterns that lacked (002) peaks. The platy graphites, despite looking quite distinct in the TEM from the well-graphitized onions, were generally lumped in as onions in earlier SEM classification, but their properties were not extensively discussed in previous TEM-based works (Bernatowicz et al. 1996; Croat et al. 2005). These discrepancies in earlier graphite classifications illustrate the need for a better measure for the degree of graphitization.

A brief explanation of the structure of graphite is required to move beyond nebulous external morphology descriptions (onions and cauliflowers) towards more quantitative measures. The term graphite is loosely used to describe various forms of carbon (e.g., graphite spherules, plate-like graphite, filamentous graphites such as carbon nanotubes and graphite whiskers, and C_{60} and other fullerenes; Jaszczak 1995), all of which are comprised of two-dimensional graphene sheets (C bonded in a hexagonal network) that are then stacked in various ways. The weak interlayer bonding between adjacent graphene sheets allows these numerous distinct structures to form, and large variations in the interplanar spacing (3.1 Å < d_{002} < 3.9 Å) are permitted. The fundamental building block of all these carbonaceous material is a basic structural unit (BSU), namely a single crystal of graphite (hexagonal, a = 2.46 Å, c = 6.7 Å) characterized by its lateral dimension (L_a), c-axis dimension (L_c or the number of graphene sheets stacked), and the interplanar spacing along the c-axis (d_{002}). As graphitization of carbonaceous materials proceeds, La increases from ~1 nm to several hundreds of nm, Lc increases from a 1–3 stacked graphene sheets to many, and d_{002} approaches 3.35 Å. The lateral dimensions of BSUs in onion and cauliflower graphites have been inferred from Raman spectra (Wopenka and Pasteris 1993; Zinner et al. 1995). Cauliflower graphites show significantly higher disorder than onions, as seen in the relative intensities of ordered and disordered Raman peaks and in the ordered peak width. From these data, the lateral dimensions of the coherently scattering domains were inferred for two cauliflower (6 nm < L_a < 14 nm) and 5 onion (14 nm < L_a < 25 nm) graphites (and these BSUs were assumed to be roughly equiaxial with similar L_c values). The nanocrystalline cores seen in many onions were likely not measured by Raman independent from the more well-graphitized rims. However, the size of these nanocrystalline BSUs has been estimated from TEM diffraction and modeling to be 3 nm < L_a < 4 nm, but with no (002) stacking (L_c is undefined) (Bernatowicz et al. 1996; Fraundorf and Wackenhut 2002). The average interplanar spacing (d_{002}) have been determined in the present work from selected area diffraction patterns, by calibrating the d_{002} spacing to known (100) and (110) in-plane spacings (which do not vary significantly). The higher density KFC1 graphite spherules have slightly larger d_{002} values than the 3.35 Å spacings in ideal graphite, with onion and platy graphites showing similar d_{002} spacings (3.49 ± 0.05 Å from 17 measurements), whereas cauliflowers have slightly larger values (3.57 ± 0.10 Å from 10 measurements). The lower-density KE3 graphites also show slightly larger d_{002} values (3.62 ± 0.05 Å from 14 measurements) as would be expected from a lower density phase, despite being more similar in appearance to the KFC1 platy graphites. The spread in interlayer spacings within an individual graphite, as reflected

in the (002) peak width, is not well determined, since variations in the film exposure conditions can alter the apparent electron diffraction peak widths.

Since ordering in poorly graphitized carbonaceous materials is manifested at different length scales, the above description of differences in the BSUs of onions and cauliflowers gives an incomplete measure of the degree of graphitization. Graphitization of carbonaceous material normally proceeds first by the mutual rearrangement of adjacent BSUs without much alteration of the individual BSU size (L_a or L_c). The length scale over which adjacent BSUs are roughly aligned is described in terms of its microtexture or the degree of local molecular ordering (LMO). The size of LMO domains can be estimated from dark-field (002) images, which reveal discrete areas in which BSUs are roughly aligned with each other. Due to the small size of individual BSUs (~10 nm), BSUs within a given domain will remain bright when their orientation is parallel to the beam direction within ~10° (Oberlin 1989). The differences between onion, platy turbostratic, and scaly cauliflower graphites can be determined in a semi-quantitative manner based on the size of the (002) dark-field domains. These LMO domain sizes are clearly different among the graphite types, as seen in typical dark-field (002) images from the onion, platy, and scaly types (Fig. 3.) Although graphites were often classified based on their distinctive appearance in bright-field images, these are reinforced by use of dark-field imaging which can allow semi-quantitative measurements of the degree of graphitization.

Relative Abundances and Size

About 15% (by volume) of the material in the KFC1 residue is graphitic, with the rest predominantly consisting of 3–5 μm amorphous silicates with an average composition of $Si_{95}Al4Fe_1$ (O content not quantified). The vast majority of the graphitic material is isotopically anomalous. Before making any comparisons between previous SEM/SIMS studies and TEM-based studies on different populations of KFC1 graphites, one must first reconcile the TEM morphological types seen (e.g., onions, platy, scaly, etc.) with the earlier SEM-based classification (onions and cauliflowers). Figure 4 compares the SEM-based and TEM-based classification of presolar graphites found in the KFC1 residue. Slightly different categories are used, with the addition of the platy turbostratic category (as described above). Many of the platy graphites were apparently classified as onions in SEM studies due to their relatively smooth outer surfaces. For example, most KE1 graphites were considered onions in SEM studies (Hoppe et al. 1995), but TEM cross-sections of their interiors in comparable KE3 graphites look quite turbostratic and are more similar to the platy graphites (Croat et al. 2003). However, the platy graphites are generally larger than onions and there are

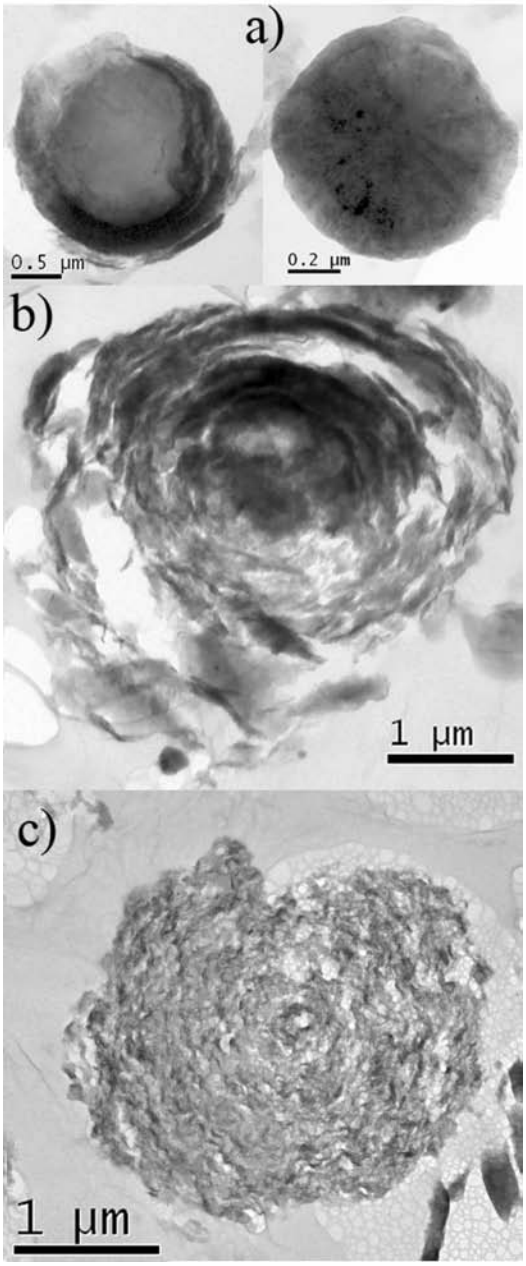

Fig. 2. a) Highly graphitic onion graphites with (left) or without (right) a nanocrystalline core having regularly stacked graphene sheets which form a dense concentric shell structure with a smooth surface. b) Platy graphites with continuous concentric layers and a relatively smooth surface and c) scaly graphite with short, curved and discontinuous (turbostratic) concentric layers and cauliflower-like surface.

obvious morphological distinctions when graphite cross-sections are observed in TEM (see Fig. 2). There are also a few types of graphites seen in TEM that are not included in Fig. 4, including several hundred crystalline/ polycrystalline graphites (N = 174 or ~9% by number overall), all of which have thus far lacked isotopic anomalies in NanoSIMS measurements (N = 4). These contain large crystalline

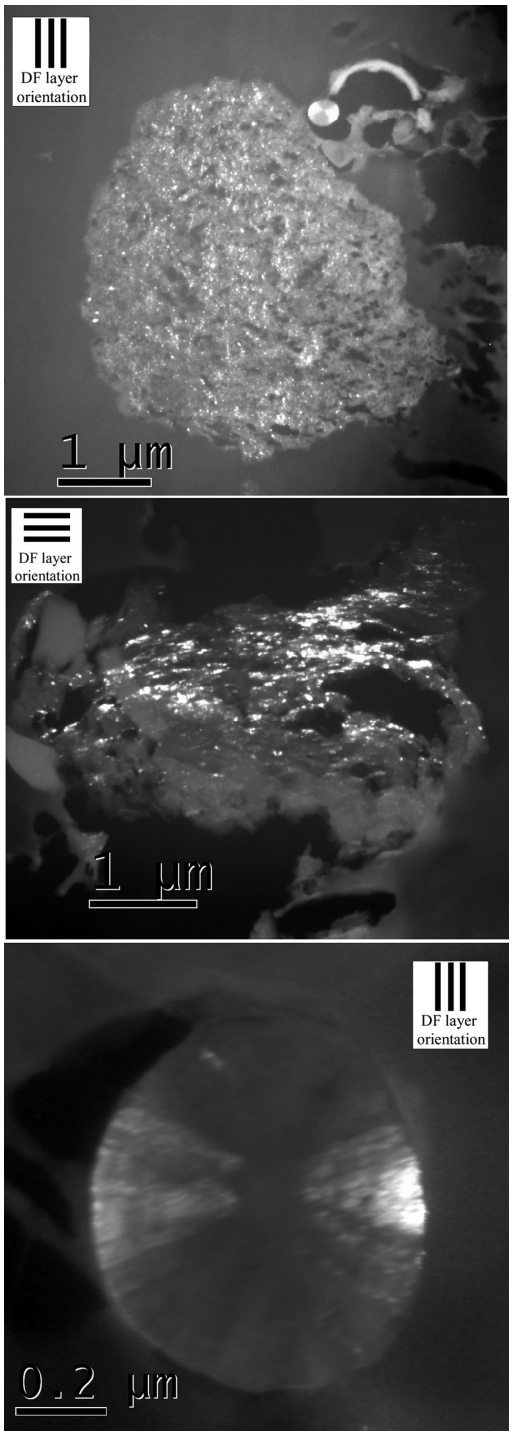

Fig. 3. Dark-field images taken from the (002) graphite spot from various morphological types. a) Scaly cauliflower. b) Platy graphite. c) Well-graphitized onion. The alignment orientation of the BSUs in bright regions is indicated by the black markers. The LMO domains in scaly graphites are equiaxial and generally less than <50 nm, whereas domains in platy graphites are typically elongated, with average dimensions of 110 nm by 60 nm. In well-graphitized onions, the domains are larger and typically >100 nm in both directions.

domains (100 nm – 1 μm+) and thus have spot diffraction patterns rather than the rings formed by smaller domains in the presolar graphites. There are also aggregates apparently consisting of multiple graphites either intergrown or cemented together (N = 45 or ~2%) that are excluded from the Fig. 4 comparison, as these were likely overlooked in the SEM-based studies as not being particularly spherical. Additionally, some unclassifiable graphite fragments (N = 227 or ~12% by number) that were damaged during ultramicrotomy are not included.

In the TEM studies of sliced graphites, all graphitic material in the field of view was classified, so the relative abundances by number in Fig. 4 should roughly match those of the overall population. As mentioned in the Experimental section, there is the possibility of observing multiple slices from the same graphite, which could lead to overcounting in the number abundance of the larger platy turbostratic and cauliflower graphites (due to higher likelihood of multiple slices from large grains). The presence of significant numbers of platy turbostratic and scaly graphites with apparent lower density (gaps within the internal structure) is somewhat unexpected in the dense KFC1 fraction (2.15–2.20 g/cm). However, larger, less dense grains, such as the 2.2 μm median diameter cauliflowers, diffuse more slowly (D ~ 1/R as described by Stokes-Einstein relation), making them more difficult to separate during centrifugation.

The size distribution of all KFC1 graphites (predominantly onions), as estimated from SEM studies, is plotted in Fig. 5a (Amari, unpublished data[1]). We do not have separate size data on unsliced platy turbostratic or scaly graphites, nor can these be easily obtained since the underlying morphological distinctions are only clear in TEM. However, we can reconstruct the true size distributions of each morphological type indirectly from the sizes of sliced graphites measured in TEM. We assumed that, prior to slicing, the graphite sizes were log-normally distributed and generated a model distribution with the same number of members as our measured distributions. Then each member of the model population was sliced at a random distance from its center. The input parameters (mean and standard deviation of the underlying lognormal distribution) were adjusted until there was a good match between the sliced model size distribution and the measured TEM slice distribution (in terms of mean size, standard deviation, and visual comparison). The model size distributions of onion, platy turbostratic and scaly cauliflower graphites are plotted in Figs. 5b–5d, with peaks in the size distributions of 1.5, 3.5, and 2.9 μm, respectively. The good agreement between the actual KFC1 distribution (Fig. 5a) and that independently generated from onion sections (Fig. 5b) suggests that this method is sound. All sizes match well with the observed TEM distributions after slicing at random heights, although fewer slices were

[1]Data available at Washington University presolar grains database, Frank Gyngard (editor), http://presolar.wustl.edu/~pgd/.

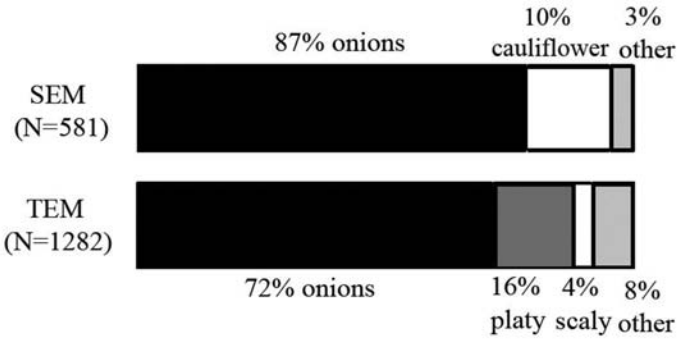

Fig. 4. Relative abundances of different graphite morphological types in KFC1 residue population as classified by TEM and SEM studies (SEM data from Hoppe et al. 1995).

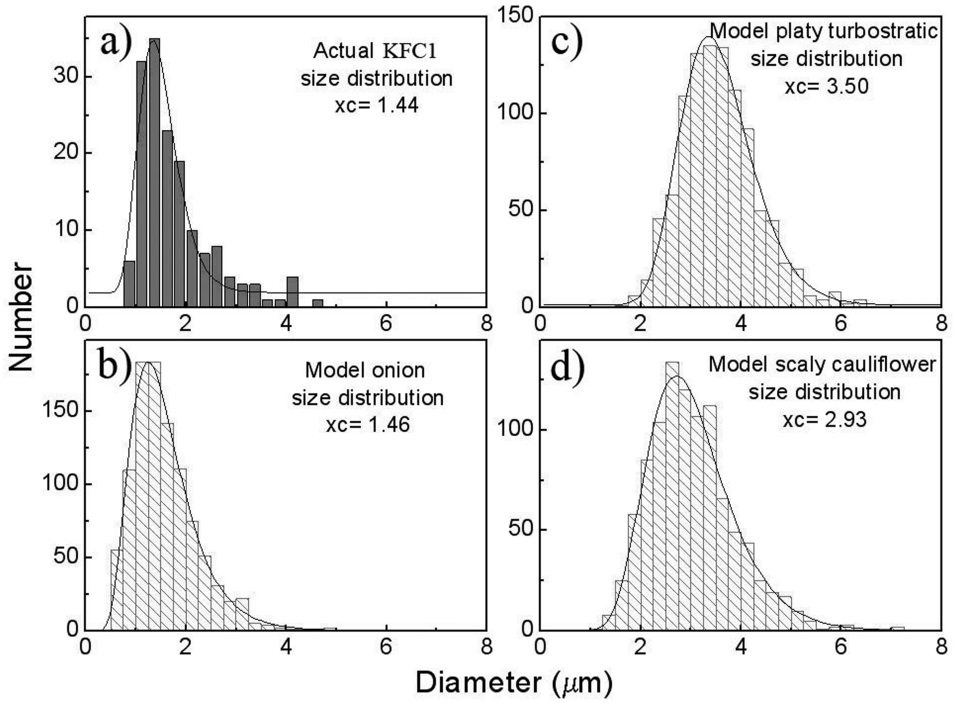

Fig. 5. a) Actual overall KFC1 graphite size distributions (Amari, unpublished data) and model size distributions reconstructed from slice diameters for (b) onion, (c) platy and (d) scaly graphites. Log-normal fits to the distributions are also shown (with x_c indicating the center of the curve).

typically observed at the smallest sizes (<0.25 μm), likely due to the inability to identify such small fragments.

Internal Carbides within Platy Turbostratic Graphites

As found previously within onion graphites (Croat et al. 2005), refractory carbides are commonly found within platy turbostratic graphites (Fig. 6a). Textural considerations and variations in carbide composition within the same graphite indicate that carbides formed first and were then incorporated into the graphite, rather than forming later by exsolution (Bernatowicz et al. 1996). For example, in some highly graphitic onions, there is strong evidence of carbides acting as nucleation centers for the graphite. When a carbide was found within a highly graphitic onion slice, 63% of the time it was found directly in the center, which can be precisely located due to the concentric graphitic cages in these structures, whereas a randomly located carbide would be central about 1% of the time (Bernatowicz et al. 1996). The refractory carbides within platy turbostratic graphites have an average size of 21 nm and ranged from 7 to 75 nm. Despite the significantly larger size of the platy turbostratic graphites (~2.3× larger than onions), the internal carbides were similar in size to those found within onion graphites (e.g., Fig. 5 from Croat et al. 2005), and so there is no direct scaling between the growth of the two kinds of phases. This suggests that the refractory carbides in both types of graphite morphologies could have formed under similar p,T

conditions, whereas later during the period of graphite growth the conditions in various parcels of gas diverged. The minimum size at which these grains can be easily detected (~5 nm) is considerably below the peak in the size distribution, so instrumental effects probably do not significantly alter the observed distribution. Carbides were found within 9% of platy slices examined (19 of 208), a comparable frequency to that found within onions. Phase identification using SAD and/or microdiffraction patterns was done to confirm that these internal grains were indeed carbides (face-centered cubic, Fm3m), often using a single major zone ([001], [011], or [111]) as the basis for the identification. Carbides were identified in about half of the platy graphites with internal grains (11 of 19), whereas the remainder were assumed to be carbides on the basis of their chemical compositions. The lattice parameters for the carbides were 4.44 ± .04 Å, which is slightly higher than that of pure synthetic TiC (4.33 Å) and presumably increased due to the trace elements present (e.g., Zr). With an average Zr content of ~16 at% (metals basis), based on Vegard's law and the reported lattice parameters of TiC (4.33 Å and ZrC (4.69 Å), one would expect a lattice parameter of ~4.4 Å. Other Ti-rich phases (one TiC_2 and four rutile grains) were found previously in onion graphites (Croat 2007), but the more common rutile is clearly chemically distinct from refractory carbides (with higher O, Cr and Nb concentrations).

Although most graphite sections (~90%) contain no refractory carbides, there are six distinct sections of platy graphites that each contains significant numbers of carbides in a single slice (from 6 to 28 carbides; see Fig. 6c.). None of these appear to come from the same graphite, based on differences in the areal fraction of carbides, on their Zr and Mo content, and when available on their $^{12}C/^{13}C$ isotopic ratios. The carbide volume fraction estimated from these graphite sections range from 40 to 900 ppm, based on the volume fraction of carbides within the observed ~100 nm thick section. These abundances imply that as many as ~1000 carbides were present within certain platy graphites. Such high carbide densities have been seen before in KE3 SN graphites (e.g., 384 different carbides have been measured in slices from KE3e11 of an estimated 1500 carbides that exist in the entire graphite).

From the large fraction of graphites that do not contain carbides, it is clear that these high TiC abundances are not typical. However, determinations of the TiC abundance relative to graphite or the fraction of graphites containing TiCs are complicated by the fact that these are observations of an ensemble of single slices rather than serial sections of entire individual graphites. We can estimate the average carbide abundance from simple models, wherein carbides of an average size (~25 nm) are randomly dispersed within a graphite at the maximum of the size distribution (3.5 μm for platy graphites), with an ensemble of ~100 nm sections taken at random heights through this model graphite (excluding 10% of the small sections at the ends lost as fragments). If we adjust the number of carbides to match the fraction of graphite sections that contain no carbides (~90%), we find that a maximum of ~3 carbides could appear in an "average" graphite, which translates into an upper limit of ~1 ppm on the average carbide volume fraction relative to graphite. Were the average carbide ppm higher than this, then more than 19 of the 208 platy slices observed would have contained carbides. This result, combined with the much higher TiC abundances inferred from certain graphites discussed above, suggests that there is a wide variability in the number density of carbides present in the gas from which the graphites condense.

Given the apparent variability in relative TiC abundance, determining the fraction of graphites that contain carbides from an ensemble of slices is problematic. However, some observations suggest that the fraction containing carbides is considerable higher than the 10% which are confirmed to have internal grains in a single slice. For example, as mentioned above, onion graphites without nanocrystalline cores appear to heterogeneously nucleate on refractory carbides, implying that at least in this subtype the carbide-containing fraction of graphites is 100%. Further, when all serial sections from an entire turbostratic KE3 graphite are observed, in all of 12 cases studied to date internal refractory carbides were found, with a single graphite sometimes containing many hundreds of carbides. This suggests that the more turbostratic types (platy and scaly ones) are also very efficient at capturing and preserving any higher temperature condensates that are already present when they form.

Chemical Composition of Internal Refractory Carbides

Refractory carbides found within platy turbostratic graphites are predominantly TiC grains (FCC, 4.44 Å), which normally contain V, Fe, Zr, Mo, and often Cr and Ru. O, Si, and Ca peaks are also present, but are attributed mainly to the graphite and substrate rather than the carbide. Table 1 summarizes the minor element content of the refractory carbides found within the 19 carbide-containing platy graphites. Very high concentrations of s-process elements (Zr, Mo and Ru) are found, far in excess of the solar values (for reference, a solar carbide would have composition $Ti_{99.35}Zr_{0.46}Mo_{0.11}Ru_{0.08}$). ZrC (Fm3m, 4.69 Å) are isostructural with TiC, allowing complete mutual solid solution with TiC, and in fact one such Zr-enriched carbide without measurable Ti was found. Mo also has a high solubility (up to 85% Mo) in Mo-Ti-C (Upadhyaya 1996), and concentrations up to 34% are seen in synthetic carbides. Details on the Ti-Ru-C and Ti-Fe-C ternary diagram are not available, but concentrations up to 18 at% Ru and ~20 at% Fe are found in TiCs. Fe levels higher than this would

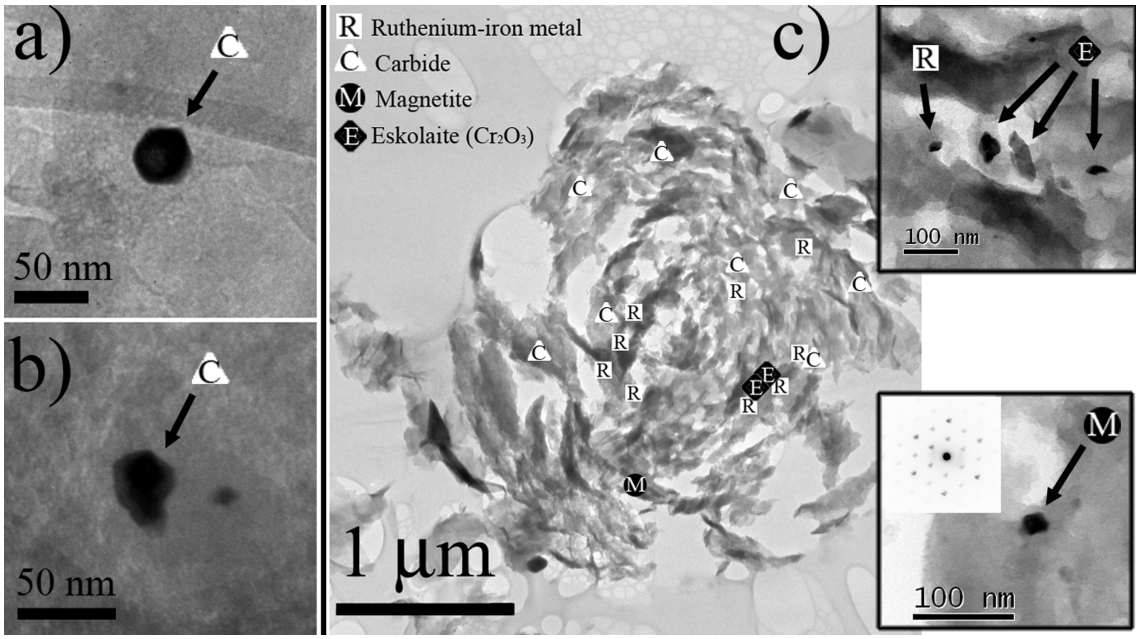

Fig. 6. a) Example of an euhedral TiC within central region of platy graphite. b) TiC without s-process elements within center of scaly graphite. c) Platy graphite with positions of various internal grains indicated by symbols and inset images of internal metallic RuFe and eskolaite (top) and magnetite (bottom) along with its [111] diffraction pattern.

Table 1. Minor element content of refractory carbides within platy graphites.

Element	% of TiCs w/detectable levels	Average at% [1]	Std. dev. (at%)	Max. at%
Zr	89%	22.8%	24.1%	69.6%
Mo	84%	13.5%	5.9%	33.8%
Ru	42%	2.9%	4.8%	17.9%
Fe	100%	4.5%	4.4%	15.0%
V	89%	3.4%	3.1%	12.7%
Cr	47%	1.2%	1.2%	3.8%

[1]All concentrations are atomic percent metals basis (including all metals present but excluding C).

Table 2. Number and type of internal grains in four RuFe-containing platy graphites.

Ref #	# TiCs	# RuFe	# TiC/ RuFe	Other phases
1	9	9	1	3 CrO (cubic)?, magnetite; RuFe/kamacite intergrowth
2	6	3	1	2 Cr_2O_3 (eskolaite)
3	11	1	0	None
4	32	7	0	2 Cr_2O_3 (eskolaite)

typically indicate metallic iron-nickel subgrains (kamacite or taenite), which were commonly found epitaxially grown onto TiC surfaces within SN graphites and in one instance were also found on TiCs within a KFC1 onion graphite. Low V concentrations were found in many carbides, with an average V/Ti of 0.06, well below the V solid solubility limit ($V/Ti_{max} \sim 0.5$), and also lower than the values found in TiCs within SN graphites ($0.07 < V/Ti < 0.2$). V/Ti ratios in TiCs may be strongly affected by chemical fractionation during condensation, since VC is a lower temperature condensate than TiC. Up to 4 at% Cr was observed within KFC1 carbides (lower than ~20 at% limit), whereas higher Cr concentrations have only been found in rutile (TiO_2) grains from four different onion graphites (Croat 2007). No correlations are found between the s-process element content and the trace concentrations of the other elements.

As discussed in Croat et al. (2005), the high s-process element content in most carbides (17 of 19 graphites) is an indicator of formation in an AGB carbon star environment. If we can properly account for chemical fractionation during condensation or show that it is minimal, then we can compare the elemental ratios of s-process elements measured within carbides (e.g., Zr/Ti or Mo/Ti ratios) with astronomical observations of AGB and post-AGB stellar spectra. One potential indicator of the degree of chemical fractionation is the Zr/Mo ratio. This ratio should be less variable than those involving Ti in AGB environments since both Zr and Mo are co-produced through the s-process. Astronomical measurements of Zr/Mo ratios vary from solar (Zr/Mo = 4.6) in normal M/K giants, but decrease by ~2× in S and SC giants (Abia and Wallerstein 1998). However, larger deviations in Zr/Mo ratios are seen among the carbide compositions, ranging from 0.01× to 4.4× of the solar value, which is taken as evidence of chemical fractionation of Zr with respect to Mo. Since ZrC is substantially more refractory than MoC or TiC, high temperature condensates are relatively Zr-rich whereas carbides forming later at lower temperatures are

more Mo-rich, and both types are observed among the refractory carbides. Carbides from 10 of 19 platy graphites are significantly Mo-rich (Zr/Mo < 1), suggesting later formation after available Zr had already condensed in other grains. We also found one high temperature ZrC condensate without any detectable Ti or Mo. Thus, the fractionation evident in the Zr/Mo ratios suggest that Zr/Ti ratios will not be a good measure of the degree of s-process enrichment.

There are several arguments against significant chemical fractionation in the Mo/Ti ratios, and therefore these more accurately reflect the degree of s-process enrichment in the gas from which the carbides condensed. First, the predicted condensation temperatures of the stable carbides TiC, ZrC, and MoC can be used as a guide, which have been computed over a range of reasonable pressures and C/O ratios (Lodders and Fegley Jr. 1995). ZrC has a higher condensation temperature than MoC or TiC over a wide range of C/O ratios and pressures, leading to the fractionation behaviors already mentioned. With solar abundance of the metallic elements, the MoC condensation temperature is 91–97% of that of TiC over the ranges (1.05 < C/O < 2 and −2 < log P (in bars) < −15; see also Table 2 from Croat et al. 2005). However, in the s-process enriched environments of AGB stars, the MoC condensation temperature will rise relative to TiC, eventually exceeding it. At a ~30× solar s-process enrichment (which is the maximum amount astronomically observed in AGB carbon stars), the predicted MoC and TiC condensation temperatures are very close (within ~20–30 °C; Lodders and Fegley 1995). Along with these predictions, several other arguments against Mo fractionation come from observed elemental ratios within the carbides. Even with large variations in the Zr/Mo ratio (presumably reflecting equilibration with the gas at different temperatures), the Mo/Ti ratios vary little and are consistently high. If Mo were fractionating relative to Ti, one might expect to see differences in Mo/Ti between higher T condensates (Zr/Mo > 1) and lower T condensates (Zr/Mo < 1). Also the Mo/Ti ratios from multiple carbides found within the same graphite are self-consistent, whereas their Zr/Ti ratios can be quite variable. Finally, we do have many examples of carbides within Murchison KE3 graphites which condensed in SN ejecta from a gas with Mo/Ti ratios that likely did not deviate greatly from the solar value (solar Mo/Ti atomic ratio ~0.0011). Zr or Mo were never detected in hundreds of larger KE3 SN carbides (Croat et al. 2003), and some grain compositions were even constrained to having slightly subsolar Zr/Ti and Mo/Ti ratios. This gives us further evidence that chemical fractionation does not significantly increase Mo/Ti ratios.

The degree of s-process enrichment, as reflected in the Mo/Ti ratios from carbides within all of the platy carbide-containing graphites, is plotted in Fig. 7. For comparison with astronomical observations of these ratios, we express these as $\log((EL/Ti)_{observed}/(EL/Ti)_{solar})$ or [EL/Ti]. So as to not skew the distribution towards graphites with higher TiC abundance,

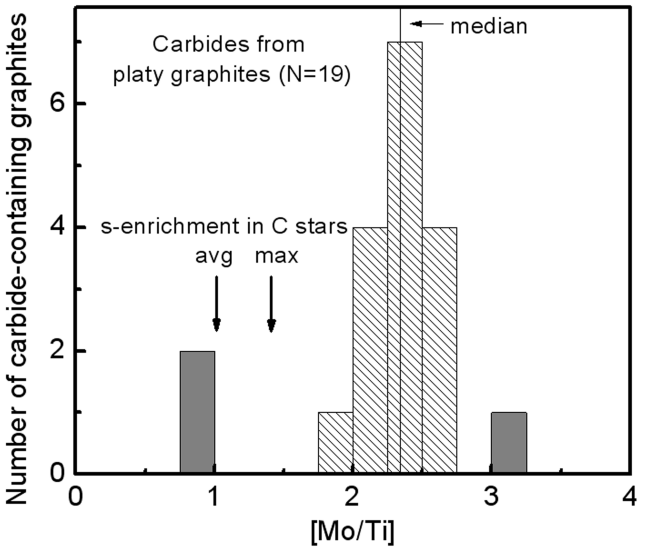

Fig. 7. [Mo/Ti] ratio (defined as $\log(Mo/Ti)_{observed}/\log(Mo/Ti)_{solar}$) from EDXS of refractory carbides found within platy graphites. Filled bars are derived from detection limits (e.g., two with low [Mo/Ti] have no detectable Mo and one at high [Mo/Ti] has no detectable Ti). S-enrichments from C stars ([ls/Ti] with ls being the mean of Y and Zr) are derived from Abia et al. (2002).

when a graphite contained multiple carbides an average single carbide elemental ratio was chosen for inclusion. The s-process enrichments in carbides within platy graphites are uniformly high: the median enrichment is ~219× with a mean value of ~170× and a range from ~6× to ~1200×. Roughly 90% of these carbides (17 of 19) have s-process enrichments that clearly exceed the maximum enrichment (~30×) observed in a large sample of AGB stars (derived from Abia et al. 2002). The astronomical s-process ratios are derived from light s-process element ratios (an average of Y and Zr) with respect to M (an average of Mg, Si, S, Ca, and Ti abundances; Abia et al. 2002), and had to be slightly adjusted based on Ti abundances from the Utsumi (1985) study to enable direct comparison with our elemental ratios. One carbide was observed to have an s-process enrichment above 1000×, but the absence of measurable Ti results in large uncertainties such that this carbide is not distinguishable from others in the high [Mo/Ti] group. For the rest of the carbides, the experimental errors in the Mo/Ti EDXS ratios from counting statistics and the k-factor determination are relatively small (15–50%) given the large magnitude of the enrichments. Thus, the [Mo/Ti] plot is effectively bimodal with all but two platy graphites falling in the s-process enriched group.

Other Internal Phases Found within Platy Graphites

There is a distinct subclass of platy graphites that contain metallic RuFe grains along with a high number density of s-process enriched carbides (Fig. 6c), and in 3 of the 4 cases

internal oxide grains including magnetite (Fe_3O_4) and eskolaite (Cr_2O_3). These 4 platy graphite sections were relatively large, with an average section diameter of 3.3 μm, and also had high TiC abundances (comprising 4 of the 6 graphites mentioned above). Table 2 summarizes the number and types of grains found in each of these platy graphites. The internal TiC grains within the RuFe-containing graphites (containing from 6 to 32 in each slice) were 17 nm on average, yielding a TiC abundance relative to graphite ranged from 40 to 70 ppm (these comprise four of six graphites mentioned earlier as having high TiC abundance). All of the refractory carbides fall in the s-process enriched group (high [Mo/Ti]), with an average composition of $Ti_{70}Mo_{15}Zr_7Ru_7$ (along with trace amounts of Fe and Cr; C not quantified). They have slightly less Zr content on average (having [Zr/Ti] of 1.4 as opposed to 1.8 average from all carbide-containing platy graphites). Several carbides from each of the four graphites were indexed to ensure that these Ti-rich grains were in fact TiC (FCC, a = 4.46 ± 0.05 Å).

Each of these graphites contains from 1 to 10 internal RuFe grains, with an average size of 16 nm (comparable to the TiC sizes). EDXS show mainly Ru and Fe, with an average Fe/Ru atomic ratio = 0.42 (ranging from 0.16 to 0.74). The grains also contain significant amounts of Ca (2–16 at%), Cr (4–7 at%), Ti (1–3 at%) and occasionally Al (6–8 at%), although the Ca and Cr may be from contributions of the graphite background. Several different Ru-rich phases were identified within these platy graphites using electron diffraction patterns. Graphite #1 contained a large ~25 nm internal RuFe grain consisting of separate attached crystal domains. Electron diffraction patterns (of the [2 −1 −1 0], [1 −2 1 −3], and [0 1 −1 1] zones) were indexed to a hexagonal structure (a = 2.8 ±0.1, c = 4.5 ± 0.1; slightly larger (~8%) than reported values for hexagonal RuFe). In addition, patterns from the other (underlying) domain in the same grain matched the [112] and [113] zones of a small unit cell cubic structure (a = 3.16 Å; presumably kamacite). At one high symmetry orientation diffraction patterns showed correspondence between the [−1 1 1] cubic zone and the [2 1 −1 0] RuFe hexagonal zone, suggesting an epitaxial relationship between metallic RuFe and kamacite. Along with this composite grain, 3 other RuFe grains within this graphite were identified as single crystal hexagonal phases on the basis of distinctive hex patterns (e.g., [0 1 −1 0] or [1 −2 1 −3]). A different RuFe phase was found in graphite #2, with two separate RuFe grains indexed to the body-centered cubic structure (a = 3.05 ± .05 Å). This is unexpected, because the solubility limit for Ru in the cubic phase is quite low (~6 at%). A single RuFe grain from RuFe-containing graphite #3, although not conclusively identified, is consistent with the hexagonal phase and inconsistent with the cubic. None of the 7 RuFe grains from the graphite #4 were indexed, although they are compositionally very similar to the others. In addition, two of the four graphites (#1 and #2) also contain a chemically distinct TiFeRu phase (with similar metals basis compositions of $Ti_{34}Fe_{23}Ru_{23}Ca_9Mo_9V_2$ and $Ti_{33}Ru_{29}Fe_{26}Mo_5Ca_5V_2$), which in graphite #1 was found to be two separate crystal domains. The [001] fcc zone of TiC was found parallel to a [011] bcc zone and, at 45° tilt away, the [011] fcc zone (again of TiC) was parallel to a [001] bcc zone, indicating a well-defined orientation relationship wherein one phase likely grew epitaxially on the other. However the identity of the second phase intergrown with TiC (a 4.4 ± 0.2 Å RuFe-rich phase, apparently body-centered cubic) is unclear, since known RuFe-containing phases are either hexagonal or bcc with a smaller unit cell.

Several internal grains in the RuFe-containing graphites were found to be oxides, which is unexpected given that graphite formation generally requires C > O. These were all closer to the center of the graphites slices (e.g., true internal grains), rather than peripheral grains which could be attached matrix minerals. In three of the four graphites, we identified Cr-oxides (mainly eskolaite Cr_2O_3) and also one instance of magnetite (Fe_3O_4). Two eskolaite grains were found in both graphites #2 and #4, with an average diameter of ~50 nm (Fig. 6c). Electron diffraction patterns from all four grains were indexed to the trigonal crystal structure (a = 5.1–5.3 Å, c = 13.9–14.4 Å; 3–7% higher than reported values). From each grain 3–7 major zones were identified, including {−1 2 − 1 0}, {0 1 −1 0}, {−1 −1 2 0} and {1 −1 0 1} zone axis patterns. Although rare, the eskolaite phase was also found in a cauliflower graphite slice unassociated with the carbide or RuFe phases. Several small (~50 nm) internal Cr-rich grains were also found near the center of graphite #1, and these indexed not to eskolaite, but rather to a cubic phase. The [111], [113] and [011] zones were found at the correct intrazonal angles for a face-centered cubic structure with 7.4 ± 0.1 Å lattice parameter. Although this appears to be the known CrO cubic phase, the lattice parameter is significantly smaller (11%) than the reported values (Pierson 1996). A ~30 nm magnetite grain with chemical composition $(Fe_{91}Ti_7Cr_2)O$ was found toward the interior of graphite #1 (600 nm from surface; Fig. 6c), and thus it is more likely to be presolar and less likely to have been part of the host meteorite matrix which might be found stuck onto the graphite's outer surface rather than embedded. The grain was confirmed to be face-centered cubic with a lattice parameter of 9.0 ± 0.1 Å, with diffraction patterns from the [111], [112] and [213] zones at the correct intrazonal angles. The O signal in this small grain is ~5× higher than that which would be seen from the background, a clear indication of an oxide. Taken together, these observations give a conclusive identification as magnetite. Despite being located well within the interiors of these graphite slices, it is possible that these oxides do not originate from the same circumstellar outflows that produced the graphites. For example, the magnetite grain could have formed by later oxidation of a pre-existing metallic iron grain

(during parent body or laboratory processing). However, many internal metallic iron grains (kamacite or occasionally taenite) are found within KFC1 graphites having survived in similar conditions, calling this scenario into question. Magnetite is also reported as a common constituent of the Murchison matrix (1.2 wt%; Hyman and Rowe 1983), so it is possible that these grains could be transferred onto the slice from the grain exterior during ultramicrotomy rather than being indigenous. A similar magnetite grain (with a = 8.9 ± 0.1 Å) of composition $(Fe_{96}Cr_4)O$ was found at the periphery of a different platy graphite, and may be of matrix origin. The origins of the oxide grains present (especially the larger Cr-oxides) will likely be discernible with new information from planned oxygen isotopic measurements.

NanoSIMS isotopic measurements of C and O have been performed on graphite #3, resulting in $^{12}C/^{13}C = 240 \pm 4$ (2σ errors) and solar oxygen isotopic ratios within errors ($^{16}O/^{18}O = 469 \pm 57$, ^{17}O not measured). This graphite contained a single RuFe grain and numerous carbides, but no oxide grains and thus it sheds no light on the origins of the oxides. The eleven refractory carbides within this graphite were s-process enriched with [Mo/Ti] = 2.39 ± 0.18 (~245× enriched from the solar ratio), but showed little Zr. Three of the carbides (those with the higher overall number of counts) had measurable Ru, which again is evidence of strongly s-process enriched compositions hundreds of times the solar ratios ([Ru/Ti] = 2.5 ± 0.2). As expected for a graphite with s-process enriched carbides, this graphite falls into the ^{12}C-rich group.

Grains of Other Phases within Platy Graphites

Along with the RuFe phases found in the platy phase assemblage mentioned above, another new FeRu phase (of approximate composition $Fe_{35}Ru_{26}Al_{19}Mo_{10}Ti_6V_3$ at% metals basis without appreciable O) was found within a platy graphite with a nanocrystalline core region. The lack of an oxygen peak suggests that this is a carbide or metal phase. The FeRu grain was found in the nanocrystalline core region, whereas a refractory carbide of composition $(Zr_{53}Ti_{32}Mo_{12}V_2Ca_1)C$ was found in the platy outer regions of this graphite fragment. The carbide is strongly enriched in s-process elements ([Mo/Ti] = 2.5) and has a solar Zr/Mo ratio (unlike most carbides which are Mo-rich). From the Zr-rich carbide, a [011] FCC zone pattern was found, yielding a calibrated lattice parameter of 4.5 ± 0.1 Å. Identification of the FeRu-rich phase is more tentative. Diffraction patterns from the [1 0 0], [1 0 −1], [2 0 −1], and [3 1 −1] zones clearly indicate a cubic structure (at correct intrazonal angles). However the extinctions within these zones are abnormal (e.g., no (111) at [1 0 − 1] orientation), and no analogous phases were located in the literature.

There are also two instances of suspected metallic iron among the platy KFC1 graphites, found without carbides or other associated phases. Both were found near the periphery of the graphite slices, with geometrical mean sizes of 21 and 29 nm. Unfortunately the TEM substrate failed before either could be conclusively identified with electron diffraction. However, EDXS spectra of both show essentially pure Fe without O, which is suggestive of metallic iron. Of the dozens of iron grains that have been indexed from other presolar graphites, all but two are metallic iron (either kamacite or taenite). The only exceptions were grains of cohenite (Fe_3C, orthorhombic) in a SN graphite (Bernatowicz et al. 1999) and a hexagonal carbide ($(Fe,Cr)_7C_3$) found in an onion KFC1 graphite. Similar internal metallic iron grains have previously been reported in KFC1 onion graphites (Croat et al. 2005) as well as SN graphites (Croat et al. 2003). In the SN graphites metallic iron was normally found epitaxially grown onto other TiCs, rather than as independent iron grains, whereas the reverse was true among iron-containing KFC1 onion graphites, with numerous independent iron grains and only a single TiC/kamacite composite grain. In terms of thermochemical condensation models, it is difficult to form any metallic iron grains prior to graphite without invoking a higher relative abundance of iron, such as those that would be present in certain SN zones. However, coordinated isotopic studies of these slices must be completed before their likely stellar source can be determined.

Properties of Scaly Cauliflower Graphites

From the data thus far (N = 44), scaly cauliflower graphites (those with smaller coherently scattering LMO domains discussed previously) are less likely to contain refractory carbides than the other KFC1 graphite groups. Since the carbides are typically smaller (by a factor of 3) than the slice thickness it is unlikely that this difference results from differential loss of internal grains plucked out during ultramicrotomy. Only one scaly slice was examined that contained internal carbides (Fig. 6b), with two small carbides (with diameters of 15 nm and 26 nm) near the center of the section. EDXS of the larger carbide showed a composition of $(Ti_{98}Fe_2)$ with slight Cr and higher than normal O (presumably both from graphite background). Neither carbide showed detectable s-process enrichments (with [Mo/Ti] < 0.8) of the type found in ~90% of carbides from platy or onion graphites. Diffraction patterns from the [011] and [112] FCC zones was collected from the larger carbide, yielding a lattice parameter of 4.54 ± 0.05 Å. The relative carbide abundance estimated from this slice is ~75 ppm, which is close to the median abundance across all platy graphites. However, the average carbide abundance is only ~6 ppm if globally averaged over all scaly graphites.

Although no other refractory carbides were found within 44 scaly graphites, one slice did contain two ~50 nm Si-rich grains (presumably SiC). The high Si/C ratios in EDXS indicate true Si presence, rather than possible

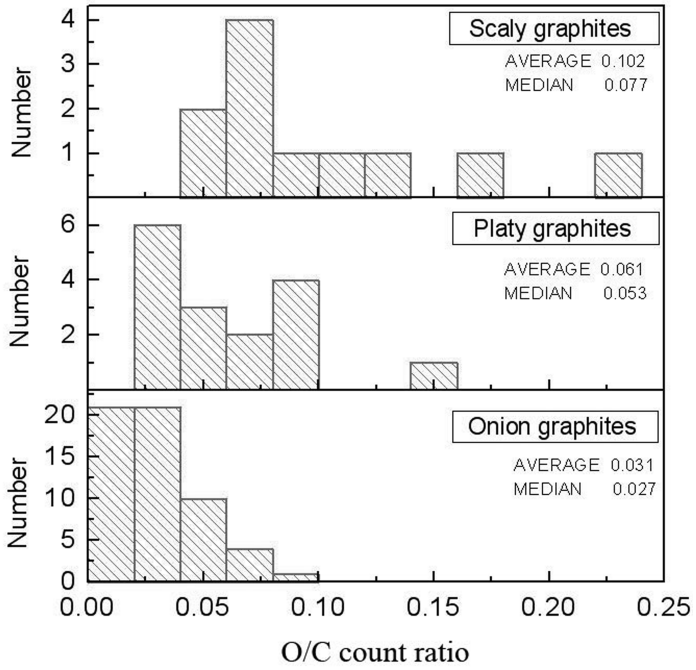

Fig. 8. Histograms of O/C count ratios from EDXS spectra of scaly, platy and onion graphites, showing a progressive increase in O content as graphites become more disordered.

contributions from the intrinsic peak, and trace amounts of Al and Mg were also visible. Given the lack of O content in these grains, they are most likely SiC. Unfortunately this grid section failed before crystallographic identification could be done. The above findings are in accord with previous studies of a single scaly LFC cauliflower graphite (Bernatowicz et al. 1991), which showed the presence of multiple TiCs without s-process enrichments, along with a Si-rich grain that was presumed to be SiC. The scaly morphology does seem to be preferentially associated with a lack of s-process elements in carbides, suggesting a SN origin due to similarity with carbides from KE3 SN graphites. However, the SiC phase is not found only in scaly graphites, as numerous examples of onion graphites with internal SiCs have been found recently (Croat and Stadermann 2006; Hynes et al. 2007).

There is an apparent trend towards higher O content in graphites with a higher degree of disorder, such as the scaly cauliflowers discussed above. Figure 8 shows the O content, as reflected in EDXS O/C count ratios, in graphites from the three different morphological groups. These EDXS measurements were taken from graphite regions over holes in the grid to minimize possible contributions from the resin or holey carbon grid. There is clearly a tendency for O content to increase as the degree of disorder within the graphite increases. EELS measurements of 22 graphites from the different morphological groups qualitatively confirmed this trend, although high backgrounds from the grid were problematic. That scaly graphites are often isotopically anomalous in O (see Fig. 9 below) shows that this increased O content is not predominantly due to infiltration of scaly graphites by resin. This observed trend is also strengthened by earlier SIMS reports of increased trace element content (mainly based on H, N, and Si) in LFC cauliflower graphites, which appear similar to the scaly ones of this study (Zinner et al. 1995). Unfortunately H is not measurable in EDXS and both N and Si measurements are complicated by high EDXS background counts, so we have yet to explore whether these elements are elevated. We also confirmed the elevated oxygen in scaly cauliflowers with NanoSIMS measurements. NanoSIMS measurements of C and O in KFC1 scaly cauliflower graphites show $^{16}O/^{12}C$ count ratios that are twice as high on average than those measured in platy and onion graphites or in the background regions of the carbon grid.

Isotopic Analyses of Different Graphite Morphological Groups

Here we present new data on the isotopic compositions of 148 onion, platy, and scaly graphites, focusing on any possible correlations of the isotopic ratios to the morphological group or other properties. Investigations into any possible correlations between the isotopic results and the types of internal grains are ongoing, and results from these detailed correlated isotopic and TEM analyses of grain-containing turbostratic graphites will be presented later. Figure 9 shows the $^{12}C/^{13}C$ and $^{16}O/^{18}O$ isotopic ratios from all KFC1 graphites by morphological type. Despite having a limited amount of material in a single ~100 nm thick slice, C

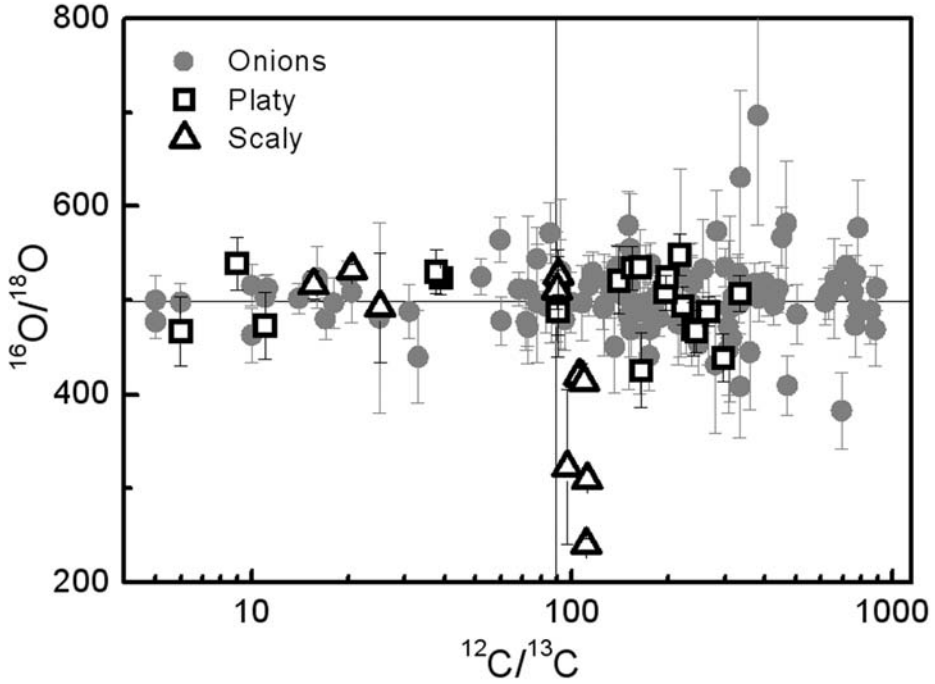

Fig. 9. $^{12}C/^{13}C$ and $^{16}O/^{18}O$ isotopic ratios from KFC1 graphites split by morphological type. 2σ O errors are shown and C errors are smaller than the symbols. No anomalies were found in $^{17}O/^{16}O$, although ^{17}O was only measured in 51 of 148 graphites.

anomalies are easily detected in the NanoSIMS (errors in C ratios are smaller than the symbols). However, attempts to measure minor element anomalies (e.g., O) are limited by insufficient counts, as seen in the sometimes large error bars. The overall C distribution for onions in Fig. 9 is in agreement with previous SIMS measurements of KFC1 graphites (which were predominantly onions; Hoppe et al. 1995; Amari, unpublished data). ^{12}C-poor and ^{12}C-rich groups are evident with all morphological types represented in both groups. There is also a pronounced gap in the $40 < {}^{12}C/^{13}C < 75$ region that contains most mainstream SiCs. In this study, 17% of onion, 26% of platy, and 33% of scaly graphites fell into the ^{12}C-poor group ($^{12}C/^{13}C < 60$), which is comparable to 24% of all KFC1 graphites in this category from the larger SIMS data sets (Amari, unpublished data). One evident trend in Fig. 9 is that the extremely ^{12}C-rich end of the distribution is apparently dominated by onion graphites, with the 30 most ^{12}C-rich grains being onions, which despite their greater number is not a random occurrence. However, this could simply reflect a different isotopic contribution from the background between the onions and the more turbostratic types. Platy graphite ultramicrotomed sections commonly have interior holes, and thus some fraction of the counts could be from the isotopically solar C grid. Under our typical measurement conditions, if ~20% of the observed C counts from a platy graphite were instead from the C background (of the grid and/or resin), then a graphite that would have fallen at the ^{12}C-rich extreme (around 800) would instead appear near the maximum $^{12}C/^{13}C$ for platy graphites (around 300). Background contributions of the same degree (20% of C signal from the grid material) would not significantly alter the isotopic ratios of graphites in the low $^{12}C/^{13}C$ group and the effects are greatly diminished away from the ^{12}C-rich extreme. Although the degree of background contributions is likely not as extreme as the worst case presented here, there is probably no significant isotopic difference between platy and onion graphites given possible dilution effects. It may be possible to estimate the degree to which background contamination plays a role by looking closely at graphite sections with high $^{12}C/^{13}C$ ratios that lay partly over holes in the holey carbon grid. If carbon counts from the substrate were in fact significant, one would expect to see more anomalous values overlying holes in the grid.

As was the case with O isotopic measurements from the larger KFC1 population (Amari, unpublished data), the O isotopic ratios of the onion and platy graphites were generally normal within errors, although 1 of 19 platy graphites has a >3σ O anomaly (slight ^{16}O excess) which may be significant. However, many of the scaly graphites measured thus far are anomalous in O, and thus appear to be isotopically distinct from the platy and onion groups. Five of nine scaly graphites show distinct oxygen anomalies, four with ^{18}O-enrichments and one with an ^{18}O deficit (all $^{16}O/^{17}O$ ratios were solar within errors). The deviations were significant, with one graphite 2.1σ away from solar O ratios and the rest with >5σ deviations). Due to the slices in which they were found and their physical properties, it is highly unlikely that all these scaly graphites are multiple slices from the same graphite. Although few scaly graphites have been studied in coordinated TEM and SIMS (9 in this study and 2 from Bernatowicz et al.

1991), all have relatively low $^{12}C/^{13}C$ ratios below 115, lower than the median of $^{12}C/^{13}C$ of the entire KFC1 graphite population. This was also noted in Hoppe et al. 1995, wherein the cauliflowers were less represented in the ^{12}C-rich graphite group. Any background effects on $^{12}C/^{13}C$ in this range would be minimal, and fails to explain why all scaly graphites are in the lower half of the $^{12}C/^{13}C$ distribution. Further, the scaly graphites have less apparent holes in their cross-sections after ultramicrotomy than the platy ones, decreasing potential problems with background contributions.

DISCUSSION

The diverse graphite morphologies outlined in the Results section were all found in the same CM2 meteorite, implying that later thermal or aqueous alteration in the meteorite or its parent body is not solely responsible for these differences. If significant thermal processing had occurred, the d_{002} spacings in the Murchison presolar graphites would probably be closer to the 3.35 Å values found in annealed graphites. Further evidence against annealing as the cause of the well-graphitized regions in onions comes from rim-core graphites. Sharp boundaries of the sort found between nanocrystalline and graphitic regions in rim-core onions could not be produced by annealing (Bernatowicz et al. 1996). Rather the morphological features of presolar graphites are primary, and to some degree reflect the graphite's formation conditions in SN ejecta and/or in outflows from AGB stars. The similarity of the more turbostratic KFC1 graphite types (platy and scaly) to KE3 SN graphites (and dissimilarity to KFC1 onion graphites most of which are of likely AGB origin; Croat et al. 2005) suggests that the turbostratic morphologies might result from the particular conditions in SN outflows. However a SN origin is not plausible for most KFC1 platy graphites. Earlier SEM-based classification lumped platy graphites into the "onion" category, and this may have been a fortuitous choice, given that no clear differences have been found in their properties (other than their obvious morphological differences apparent in cross-sectional TEM images).

The first key similarity between the platy and onion graphites is in the chemical composition of their internal carbides. The s-process element enrichments are several hundred times the solar values in both morphological types, and as argued previously these values do not appear to be strongly affected by fractionation. This is reinforced by the presence of RuFe metal grains in four platy graphites, whose growth would be kinetically inhibited in all but the most strongly s-process enriched environments. The primary utility of the s-process element ratios in presolar grains studies is to distinguish between AGB and SN stellar sources, and only secondarily to compare these ratios with those derived from astronomical observations. Models of the elemental composition of SN ejecta show that a SN origin is not consistent with the composition of most carbide-containing platy graphites. In the Rauscher et al. (2002) models, globally averaged Mo/Ti ratios are subsolar (from 9–94% of the solar value of Mo/Ti = 0.001) across various 15–25 solar mass models, and other SN models give comparable results (e.g., Limongi and Chieffi 2003). Even if refractory carbides were to condense in the most s-enriched SN zone, the maximum Mo/Ti ratios are only 3–7× solar (which occurs in the inner O/C zone), clearly insufficient to produce the enrichments observed in the KFC1 platy carbides (Heger, unpublished data[2]). These model predictions are borne out by the elemental compositions of refractory carbides found within KE3 SN carbides, which show no detectable s-process elements and in some cases were constrained to have subsolar s-process element ratios (Croat et al. 2003). In contrast, AGB stars are the source of the main s-process, which produced most of the light s elements (including Zr, Mo and Ru) that are found in the solar system. In the ^{13}C pockets at the top of the He intershell region of an AGB star, enrichments of s-only elements can be as high as 25,000× the solar ratios, although these enrichments are then greatly diluted by mixing (Lugaro et al. 2003). Astronomical observations confirm the s-process enrichment of light s-elements (usually expressed relative to Fe). These enrichments are easier to detect in post-AGB stars, and maximum enrichments of ~100× solar are observed (average of ~40× but with high variability even among similar stars; Reyniers et al. 2004). Taken together, the experimental and modeling results on s-process enrichment in various stellar sources show that most of the carbide-containing KFC1 platy graphites are formed in AGB stars.

While Zr and Mo are predominantly s-process elements, isotopic analyses show that only ~20% (5 of 26 grains) of entire KFC1 graphites exhibit isotopic evidence of s-process enrichment (namely deficits in all other isotopes when normalized to the s-only isotope ^{96}Mo; Nicolussi et al. 1998). The results are limited and more variable for Zr, but 5 of 9 showing pronounced deficits (up to –926‰) in the ^{96}Zr r-only isotope, suggesting s-process enrichment, although two others show enrichments in ^{96}Zr (Nicolussi et al. 1998). The Zr and Mo presumably come from internal carbides and the quality of the RIMS measurements of entire graphites is limited by low Zr and Mo abundance, estimated at ~10 ppm. That Mo s-process anomalies are less common than Zr ones may be a result of contamination with solar Mo, and such contamination has been used to explain isotopic results from similar RIMS studies of presolar SiCs (Barzyk et al. 2006). There is a discrepancy between the percentage of graphites attributed to an s-process enriched source based on the RIMS results on whole graphites as compared to the extreme chemical enrichments measured in internal carbides. However, much of this discrepancy might be resolved if solar

[2]Data available through Nucleosynthesis in Massive Stars website, Alexander Heger (editor), www.nucleosynthesis.org.

contamination combined with low Mo abundances are significant problems for RIMS. Although the relative abundances are quite variable, the low average carbide abundance within KFC1 graphites (estimated at a few ppm above) suggests that RIMS measurements of Zr and Mo will always be challenging.

As mentioned, the C isotopic distributions from platy graphites do not reach the ^{12}C-rich extremes seen in onions, possibly due to some dilution with solar material from the C substrate. Despite enrichments being less extreme, roughly 2/3 of the platy graphites still have ^{12}C enrichments that exceed those inferred from astronomically observations of carbon stars ($30 < {}^{12}C/{}^{13}C < 70$; Lambert et al. 1986) and many even exceed those from the most extreme post-AGB stars measured (^{12}C/^{13}C values as high as ~200; Bonacic Marinovic et al. 2007). Although the two are associated, there does not appear to be a direct correlation between the ^{12}C/^{13}C ratio and s-process enrichments, as astronomical observation of AGB stars and post-AGB stars show that the strength of the s-process enrichment differs among otherwise similar stars (Reyniers et al. 2007). Unfortunately we currently have insufficient data on carbide-containing platy graphites to investigate whether ^{12}C and s-process enrichments are well correlated. However, the extreme s-process enrichments in carbides within platy graphites suggest that these graphites also form in regions inhomogeneously enriched in the nucleosynthetic products of AGB thermal pulses (Croat et al. 2005).

Another factor that likely contributes to the increased ^{12}C and s-process element enrichments in KFC1 graphites is formation in lower metallicity AGB stars. Stellar models (Zinner et al. 2006) have shown that lower metallicity (15–30% of solar) stars can reach sufficiently high ^{12}C/^{13}C ratios at the time of the last dredge up (after which a significant number of grains will still form) to explain the C enrichments seen in most graphites from Fig. 9. AGB stellar models show that lower metallicity stars (~1/2 solar) are also good candidates to explain formation of the main s-process component, and thus a low metallicity origin could simultaneously help explain the large s-process enrichments seen within the internal carbides (Gallino et al. 1998; Travaglio et al. 2004). The only drawback of a low metallicity AGB origin for KFC1 graphites is that the necessarily reduced gas number density (of Ti and other metals) will make more difficult the already tenuous formation of carbides (e.g., see Bernatowicz et al. 2005).

For the most part O anomalies are absent from the platy and onion graphites measured, although our measurements of platy graphites did yield 1 of 19 with a slight ^{16}O excess (>3σ anomaly). None of the 119 onions showed anomalies of even this magnitude. This lack of measurable O isotopic anomalies persists even when the entire graphite is available for analysis (rather than a single slice). Only 1 of 119 KFC1 graphites (Amari, unpublished data) appears to contain a ^{16}O/^{18}O anomaly (>4σ deviation) that exceeds those variations expected for a random distribution, but its morphological type is unknown since these measurements were taken from the wider population (mostly onions). No comparable prior measurements exist for the platy population.

If these platy and onion graphites are truly predominantly from C-rich AGB stars, one would expect them to mirror the O isotopic composition of such sources. Spectroscopic O isotopic measurements have been made on N stars (Harris et al. 1987) as well as on the envelopes of post-AGB C stars, protoplanetary nebulae and planetary nebulae (Kahane et al. 1992), which are likely similar to the formation environments of these graphites. The range of O isotopic compositions seen in N stars were $550 < {}^{16}O/{}^{17}O < 4100$ for ^{17}O and $700 < {}^{16}O/{}^{18}O < 2500$ for ^{18}O (Harris et al. 1987), which for comparison fall between the group 1 and group 2 oxides from O-rich AGB stars (Nittler et al. 1997). The measurements from C star envelopes are indistinguishable from group 1 oxides, with $300 < {}^{16}O/{}^{17}O < 800$ and $300 < {}^{16}O/{}^{18}O < 1300$ (Kahane et al. 1992). It is instructive to consider whether O anomalies of this magnitude would be detectable in our specific NanoSIMS experiments on ultramicrotomed graphites were they to exist. Given the average O error magnitudes and using a 3σ criterion for considering a graphite anomalous, graphites with O anomalies falling within the ranges $430 < {}^{16}O/{}^{18}O < 650$ and $1990 < {}^{16}O/{}^{17}O < 5560$ would be indistinguishable from solar. However, if the values derived from astronomical observations are correct, the expected O anomalies are mostly outside of this undetectable range. Were these graphites to have N-star-like anomalies, they would appear anomalous in ^{18}O (typically with higher ^{16}O/^{18}O ratios). If instead these graphites were to have group 1-like anomalies, most would not be clearly anomalous in ^{18}O but would show lower than solar ^{16}O/^{17}O anomalies. Therefore, it is likely that some contamination by solar O has occurred.

One obvious difference between the KFC1 platy and onion graphites is their average size (1.5 μm for onions and 3.5 μm for platy graphites). Admittedly, there are some difficulties in determining the exact size distributions of each subtype, given that they are reconstructed from the diameters of sliced graphites. Further, there could be size selection effects due to centrifugation, but neither of these complications would likely produce a size difference of the magnitude observed. One possible explanation of both the larger size and higher degree of disorder in platy graphites is that they grew faster than onions due to higher number density of condensable carbon in the gas. If the arrival of adatoms is significantly faster than the rate of surface migration of condensed species, one would also expect a higher degree of graphite disorder. Earlier graphite growth models looking in detail at the overall KFC1 graphite size distribution also suggested that some graphites do require higher C number density (Bernatowicz et al. 1996). Most of the KFC1 size distribution (~80% of grains) could result from

allowing a small spread in the nucleation temperatures of graphites (e.g., at different undercoolings) under fairly uniform conditions. However, formation of the largest graphites (presumably the platy ones) requires much higher C number densities and/or longer deposition times. Further, if the gas number density were higher, this would necessarily increase the available time for deposition. Higher gas number densities result in stronger gas drag on the grains, which then decrease their outward terminal velocities and prolong the time interval when the C number density is sufficiently high for growth to occur. An in-depth discussion of the dynamics of graphite growth in AGB outflows can be found in Bernatowicz et al. 2005. Such higher gas number densities could be found in clumps and jets of the sort seen in inhomogeneous AGB outflows (e.g., Weigelt et al. 1998; Leão et al. 2006). As a result of this study, we have identified this subpopulation of larger KFC1 graphites that require higher C number densities as platy graphites, and suggest that their more turbostratic morphologies are another indication of their more rapid growth.

There are two properties of scaly graphites that resemble those of the KE3 SN graphites. Foremost is the prevalence of O anomalies, especially ^{18}O enrichments seen in 4 of 9 scaly graphites, which is comparable to the ~2/3 of KE3 graphites with O anomalies, almost all of which are ^{18}O enrichments (Amari, unpublished data). A further similarity is the lack of s-process enrichment in the refractory carbides, although admittedly only one example of a carbide-containing scaly graphite was found. Taken together, these two observations suggest that a SN origin is more likely for the scaly graphites. This is more clearly true for the four with large ^{18}O enrichments which imply a massive star origin (most likely SN but Wolf-Rayet is possible as well; Amari et al. 1995). There are some differences between the scaly KFC1 and turbostratic KE3 groups. The inferred TiC abundance in scaly graphites is lower (~6 ppm globally averaged over all scaly graphites) than for the KE3 SN graphites examined, although the range in SN graphites was quite large (25–2400 ppm) (Croat et al. 2003). Further, the scaly KFC1 graphites are generally more turbostratic (in terms of having slightly smaller crystal domain sizes in dark-field images) than the SN graphites, which are closer to the platy KFC1 graphites in this respect.

Based on these and previous results, we can estimate the fraction of KFC1 graphites that originate in AGB stars as opposed to those from massive stars (e.g., SNe). As mentioned above, a SN origin is most likely for the scaly KFC1 graphites (4% of total), whereas onion and platy graphites can originate in either SN or AGB stellar sources. If we assume that the grain-containing fraction is representative of the entire population (and perhaps a majority of whole graphites do contain internal grains as discussed above), we can estimate the fraction of onion and platy graphites attributable to each major stellar type. Roughly 85% of carbide-containing onion (Croat et al. 2005) and platy graphites have large s-process element enrichments indicating an AGB origin. Of the remainder, ~5% contain internal SiCs which show large ^{29}Si and ^{30}Si enrichments that necessitate a massive star origin (Croat and Stadermann 2008). The remaining 10% contain TiCs without s-process enrichment chemically similar to those found in KE3 SN graphites, so ~15% of onion and platy graphites most likely originate in SN. Thus for the overall KFC1 population (including scaly, onion, and platy graphites from Fig. 4 while setting aside the 8% of other graphites) ~19% are of SN origin with the remainder being of AGB origin. At this point, similarly detailed estimates of the stellar sources of lower density graphites (Murchison KFA, KFB, and KE3) cannot be made. However, based on the increasing prevalence of ^{18}O enrichments in the lower density fractions (e.g., 2/3 of KE3 graphites), the overall fraction of Murchison graphites originating in SNe will be higher than that of KFC1 graphites.

Although there are no clear correlation between the more turbostratic morphological groups and a particular type of stellar source, there does appear to be a link between the turbostratic morphology and the O content. The O content (as reflected in both EDXS and NanoSIMS O/C count ratios) increases as the degree of graphite disorder increases. Such correlations of degree of disorder with the presence of certain heteroatoms are well known in the field of graphitization. A required step in the process of moving from poorly graphitized carbon to graphite by annealing is the removal of heteroatoms (such as H, N, and O; Wopenka and Pasteris 1993). In studies of synthetic graphites, if the carbonaceous precursor materials are richer in O or S, the size of the resulting LMO domains is smaller (i.e., they are more disordered; Oberlin 1989). This behavior has been attributed to O promoting stronger cross-linking of aliphatic groups in the carbonaceous material, which reduces their mobility and prevents them from stacking nicely. It is not clear whether results from synthetic graphite studies that are formed via annealing have any bearing on condensation of presolar graphites in stellar outflows or SN ejecta. However, to the degree that more O is present in the condensation environment, any rearrangement of atoms as they condense onto a growing graphite spherule would be hampered by the presence of heteroatoms, leading to more disordered structures. The manner in which O is cross-linked into the turbostratic graphite structures would also minimize any isotopic exchange, leading to better retention of any O anomalies in more turbostratic graphites as opposed to onions. It is also possible that the C number density or other factors (e.g., cooling rate, amount of undercooling, etc.) are the primary determinants of the degree of disorder. Then, the increased heteroatom concentrations in more turbostratic graphites could simply be due to increase availability of sites that they can occupy. Once present, any excess O would stabilize the structure against further graphitization. Given the discovery of such correlations simply in a posteriori analyses, it is difficult to determine whether any cause-effect relationships exist.

It may not be coincidental that all of the scaly graphites have relatively low $^{12}C/^{13}C$ ratios (less than 115 and well below the median value of all presolar graphite grains). Since most of the C that creates a C star from its O-rich AGB precursor is ^{12}C from helium burning, the $^{12}C/^{13}C$ ratio increases as the C/O ratio does. Thus, lower $^{12}C/^{13}C$ ratios correlate well with higher O content, as is confirmed by spectral observations of carbon stars (e.g., Fig. 40 in Lambert et al. 1986). Such a correlation may also hold in SN ejecta, as models show high C/O and high $^{12}C/^{13}C$ in the same SN zones (e.g., He/C zone with highest C/O also has extremely high $^{12}C/^{13}C$ ratios). However, studies of isotopic anomalies in presolar grains of SN origin have shown that mixing processes within SN ejecta are very complex (Travaglio et al. 1999) which would obviously weaken any such correlations. So the lower $^{12}C/^{13}C$ ratios measured in scaly graphites imply that, in general, the environments from which they condensed would contain relatively higher amounts of O than those environments producing onions. The lower carbon isotopic ratios give an independent line of evidence suggesting that more O was present in the formation environment, possibly contributing to the higher degree of disorder in the more turbostratic graphites.

SUMMARY AND CONCLUSION

Examination of over 1200 sliced graphites from the Murchison KFC1 fraction reveals diverse morphologies among the round presolar graphites. Along with previously reported well-graphitized onions (~3/4 of population), more turbostratic (i.e., disordered) morphologies are also present, such as platy graphites and scaly cauliflower graphites. Although all morphological groups are crystallographically similar with approximately equal interlayer spacings, they are differentiated by their microtexture. Platy graphites have continuous concentric layering and well-developed lattice fringes, but, unlike onions, appear fragmented in cross-sections and have smaller local molecular ordered domains (~100 nm × ~60 nm on average). Scaly graphites are the most turbostratic, consisting of short curved and discontinuous layers lacking in long range continuity with LMO domains <50 nm. We present chemical and structural data from hundreds of internal refractory grains captured during the graphite's growth, which along with the isotopic signatures give further clues about their origins. We also report the discovery of various new phases found inside presolar graphites, such as metallic RuFe and various oxide grains (eskolaite, magnetite, etc.). Further, we present new NanoSIMS isotopic data on C and O from KFC1 graphite slices (119 onion, 20 platy, and 9 scaly).

Despite the morphological differences and their larger size, platy graphites are quite similar to well-graphitized onions in terms of their isotopic properties or the types of refractory inclusions they contain. As with KE3 SN graphites, the morphologically similar platy graphites were very efficient at capturing higher temperature condensates; in some cases dozens of internal carbides are found, although the TiC abundances are highly variable (~1 to 1000 ppm relative to graphite). However, like the well-graphitized onions, a majority of carbide-containing platy graphites (~90%) show strong s-process enrichments (~220× solar on average), indicating formation in AGB outflows rather than SNe. Metallic Ru-rich phases are also found along with carbides (and even oxides) in a subset of platy graphites, further indications of an s-process enriched source. The carbon isotopic distribution of platy graphites is also similar to onions, containing both ^{12}C-poor ($5 < ^{12}C/^{13}C < 40$) and ^{12}C-rich ($100 < ^{12}C/^{13}C < 350$) groups, with a pronounced gap in the region where most mainstream SiCs reside ($40 < ^{12}C/^{13}C < 75$). However, the platy graphites do not reach the ^{12}C-rich extremes seen in onions ($^{12}C/^{13}C$ as high as 900 for onions in this study), but this may be partly due to greater isotopic contribution from the carbon-rich substrate. Most platy graphites do exceed the maximum $^{12}C/^{13}C$ ratios that are inferred from astronomical observations of carbon stars and post-AGB stars. The large ^{12}C enrichments combined with the extreme s-process element enrichments suggest formation in a region inhomogeneously enriched in the nucleosynthetic products of thermal pulses in AGB stars. An origin in lower-metallicity AGB stars could also contribute to the increased ^{12}C and s-process enrichments, although the lower number density of metals would make carbide formation more difficult. Unfortunately we currently have insufficient isotopic data on carbide-containing graphites to know whether the s-process enrichments and ^{12}C enrichments are well correlated.

The graphites with the most turbostratic scaly morphologies appear to be distinct from both platy graphites and well-graphitized onions. Five of nine graphites show O anomalies (mainly ^{18}O excesses), suggesting a SN origin as was the case for many KE3 graphites. The scaly graphites are less likely to contain internal carbides, with only one graphite containing probable SiCs and another containing TiCs without s-process enrichment. Taken together, the properties of the scaly cauliflower graphites suggest a SN origin for most members of this rare KFC1 subtype.

The larger size of the more turbostratic graphites (both platy and scaly) suggest either higher carbon number densities or longer formation times in the environments from which they condensed, and since the two are associated both likely play a role. However, the larger and more disordered graphites cannot be ascribed to a single type of stellar source, since both AGB and SN sources are inferred based on the properties of different graphites. As graphites become more disordered, progressively increasing oxygen content is found within them (as seen in EDXS and NanoSIMS O/C count ratios). Although any causal relationships are difficult to discern, the presence of oxygen

can stabilize these grains against further graphitization and probably reflects a higher O/C ratios in their formation environments. Further interesting insights into trends in the morphology and other properties of graphites from different density fractions will likely come from planned studies of Orgueil graphites which, unlike those from Murchison, are reported to contain much larger graphites in the high density fractions and also appear to lack cauliflower grains (Jadhav et al. 2006).

Acknowledgments—We thank Roy Lewis (University of Chicago) and Sachiko Amari (Washington University) for preparing the Murchison KFC1 samples. This material is based on work supported by NASA under grants NNG04GG13G and NNX07AF98G issued through the Office of Space Science.

Editorial Handling—Dr. Ian Lyon

REFERENCES

Abia C. and Wallerstein G. 1998. Heavy-element abundances in seven SC stars and several related stars. *Monthly Notices of the Royal Astronomical Society* 293:89–106.

Abia C., Dominguez I., Gallino R., Busso M., Masera S., Straniero O., de Laverny P., Plez B., and Isern J. 2002. s-Process nucleosynthesis in carbon stars. *The Astrophysical Journal* 579: 817–831.

Amari S., Lewis R. S., and Anders E. 1994. Interstellar grains in meteorites: I. Isolation of SiC, graphite, and diamond; size distributions of SiC and graphite. *Geochimica et Cosmochimica Acta* 58:459–470.

Amari S., Zinner E., and Lewis R. S. 1995. Large ^{18}O excesses in circumstellar graphite grains from the Murchison meteorite: Indication of a massive-star origin. *The Astrophysical Journal* 447:L147–L150.

Barzyk J. G., Savina M. R., Davis A. M., Gallino R., Pellin M. J., Lewis R. S., Amari S., and Clayton R. N. 2006. Multi-element isotopic analysis of single presolar SiC grains. *New Astronomy Reviews* 50:587–590.

Bernatowicz T. J., Amari S., Zinner E. K., and Lewis R. S. 1991. Interstellar grains within interstellar grains. *The Astrophysical Journal* 373:L73–L76.

Bernatowicz T. J., Cowsik R., Gibbons P. C., Lodders K., Fegley B. Jr., Amari S., and Lewis R. S. 1996. Constraints on stellar grain formation from presolar graphite in the Murchison meteorite. *The Astrophysical Journal* 472:760–782.

Bernatowicz T., Bradley J., Amari S., Messenger S., and Lewis R. 1999. New kinds of massive star condensates in a presolar graphite from Murchison (abstract #1392). 30th Lunar and Planetary Science Conference. CD-ROM.

Bernatowicz T. J., Akande O. W., Croat T. K., and Cowsik R. 2005. Constraints on grain formation around carbon stars from laboratory studies of presolar graphite (abstract #1509). 36th Lunar and Planetary Science Conference. CD-ROM.

Bernatowicz T. J., Croat T. K., and Daulton T. L. 2006. Origin and evolution of carbonaceous presolar grains in stellar environments. In *Meteorites and the early solar system II*, edited by Lauretta D. S. and McSween Jr. H. Y. Tucson: The University of Arizona Press. pp. 109–126.

Bonacic Marinovic A., Lugaro M., Reyniers M., and Van Winckel H. 2007. Stellar population synthesis of post-AGB stars: The s-process in MACHO 47.2496.8. *Astronomy and Astrophysics* 472: L1–L4.

Clayton R. N. and Nittler L. 2004. Astrophysics with presolar stardust. *Annual Review of Astronomy and Astrophysics* 42:39–78.

Croat T. K. 2007. Rutile found within presolar graphite (abstract #5217). 70th Annual Meeting of the Meteoritical Society. *Meteoritics & Planetary Science* 42:A34.

Croat T. K., Bernatowicz T., Amari S., Messenger S., and Stadermann F. J. 2003. Structural, chemical, and isotopic microanalytical investigations of graphite from supernovae. *Geochimica et Cosmochimica Acta* 67:4705–4725.

Croat T. K., Stadermann F. J., and Bernatowicz T. J. 2005. Presolar graphite from AGB stars: Microstructure and s-process enrichment. *The Astrophysical Journal* 631:976–987.

Croat T. K. and Stadermann F. J. 2006. Silicon carbide within presolar graphite (abstract #2048). 37th Lunar and Planetary Science Conference. CD-ROM.

Croat T. K. and Stadermann F. J. 2008. Extreme ^{29}Si and ^{30}Si enrichments found in rare Murchison SiC-containing graphites (abstract #1739). 39th Lunar and Planetary Science Conference. CD-ROM.

Fraundorf P. and Wackenhut M. 2002. The core structure of presolar graphite onions. *The Astrophysical Journal* 578: L153–L156.

Gallino R., Arlandini C., Busso M., Lugaro M., Travaglio C., Straniero O., Chieffi A., and Limongi M. 1998 Evolution and nucleosynthesis in low-mass asymptotic giant branch stars. II. Neutron capture and the s-process. *The Astrophysical Journal* 497:388–403.

Harris M. J., Lambert D. L., Hinkle K. H., Gustafsson B., and Eriksson K. 1987. Oxygen isotopic abundances in evolved stars. III. 26 carbon stars. *The Astrophysical Journal* 316:294–304.

Hoppe P., Amari S., Zinner E., and Lewis R. S. 1995. Isotopic compositions of C, N, O, Mg, and Si, trace element abundances, and morphologies of single circumstellar graphite grains in four density fractions from the Murchison meteorite. *Geochimica et Cosmochimica Acta* 59:4029–4056.

Hyman M. and Rowe M. W. 1983. The origin of magnetite in carbonaceous chondrites. 13th Lunar and Planetary Science Conference. pp. 341–342.

Hynes K. M., Croat T. K., and Bernatowicz T. J. 2007. Microstructure of silicon carbides found within presolar graphite (abstract #1693). 37th Lunar and Planetary Science Conference. CD-ROM.

Jadhav M., Amari S., Zinner E., and Maruoka T. 2006. Isotopic analysis of presolar graphite grains from Orgueil. *New Astronomy Reviews* 50:591–595.

Jaszczak J. A. 1995. Graphite: flat, fibrous and spherical. In *Mesomolecules: From molecules to materials*, edited by Mendenhall G. D., Greenberg A., and Liebman J. New York: Chapman and Hall. pp. 161–180.

Kahane C., Cernicharo J., Gomez-Gonzalez J., and Guélin M. 1992. Isotopic abundances in carbon-rich circumstellar envelopes: Further iteration on the oxygen isotope puzzle. *Astronomy and Astrophysics* 256:235–250.

Lambert D. L., Gustafsson B., Eriksson K., and Hinkle K. H. 1986. The chemical composition of carbon stars. I. Carbon, nitrogen, and oxygen in 30 cool carbon stars in the galactic disk. *The Astrophysical Journal* 62:373–425.

Leão I. C., de Laverny P., Mékarnia D., de Medeiros J. R., and Vandame B. 2006. The circumstellar envelope of IRC+10216 from milli-arcsecond to arcmin scales. *Astronomy and Astrophysics* 455:187–194.

Limongi M. and Chieffi A. 2003 Evolution, explosion, and

nucleosynthesis of core-collapse supernovae. *The Astrophysical Journal* 592:404–433.

Lodders K. and Fegley Jr. B. 1995. The origin of circumstellar silicon carbide grains found in meteorites. *Meteoritics* 30:661–678.

Lugaro M., Davis A. M., Gallino R., Pellin M. J., Straniero O., and Käppeler F. 2003. Isotopic compositions of strontium, zirconium, molybdenum, and barium in single presolar SiC grains and asymptotic giant branch stars. *The Astrophysical Journal* 593:486–508.

Messenger S., Keller L. P., and Lauretta D. S. 2005. Supernova olivine from cometary dust. *Science* 309:737–741.

Nguyen A. N., Stadermann F. J., Zinner E., Stroud R. M., Alexander C. M. O. D., and Nittler L. R. 2007. Characterization of presolar silicate and oxide grains in primitive carbonaceous chondrites. *The Astrophysical Journal* 656:1223–1240.

Nicolussi G. K., Pellin M. J., Lewis R. S., Davis A. M., Clayton R. N., and Amari S. 1998. Zirconium and molybdenum in individual circumstellar graphite grains: New isotopic data on the nucleosynthesis of heavy elements. *The Astrophysical Journal* 504:492–499.

Nittler L. R., Alexander C. M. O. D., Gao X., Walker R. M., and Zinner E. 1997. Stellar sapphires: The properties and origins of presolar Al_2O_3 in meteorites. *The Astrophysical Journal* 483: 475–495.

Oberlin A. 1989. High-resolution TEM studies of carbonization and graphitization. In *Chemistry and physics of carbon,* edited by Thrower P. New York: Dekker. pp. 1–143.

Pierson H. O. 1996. *Handbook of refractory carbides and nitrides: properties, characteristics, processing, and applications*. Park Ridge, N. J.: Noyes Publications. 340 p.

Rauscher T., Heger A., Hoffman R. D., and Woosley S. E. 2002. Nucleosynthesis in massive stars with improved nuclear and stellar physics. *The Astrophysical Journal* 576:323–348.

Reyniers M., van Winckel H., Gallino R., and Straniero O. 2004. A study of the s-process in the carbon-rich post-AGB stars IRAS 06530-0213 and IRAS 08143-4406 on the basis of VLT-UVES spectra. *Astronomy and Astrophysics* 417:269–281.

Reyniers M., Van de Steene G. C., van Hoof P. A. M., and van Winckel H. 2007. IRAS 08281-4850 and IRAS 14325-6428: Two A-type post-AGB stars with s-process enrichment. *Astronomy and Astrophysics* 471:247–254.

Stadermann F. J., Croat T. K., Bernatowicz T. J., Amari S., Messenger S., Walker R. M., and Zinner E. 2005. Supernova graphite in the NanoSIMS: carbon, oxygen and titanium isotopic compositions of a spherule and its TiC sub-components. *Geochimica et Cosmochimica Acta* 69:177–188.

Travaglio C., Gallino R., Amari S., Zinner E., Woosley S., and Lewis R. S. 1999. Low-density graphite grains and mixing in type II supernovae. *The Astrophysical Journal* 510:325–354.

Travaglio C., Gallino R., Arnone E., Cowan J., Jordan F., and Sneden C. 2004. Galactic evolution of Sr, Y, and Zr: A multiplicity of nucleosynthetic processes. *The Astrophysical Journal* 601: 864–884.

Upadhyaya G. S. 1996. *Nature and properties of refractory carbides*. Commack, NY: Nova Science Publishers. 545 p.

Utsumi K. 1985. Abundance analyses of thirty cool carbon stars. *Proceedings of the Japan Academy* 61B: 193–196.

Weigelt G., Balega Y., Blocker T., Fleischer A. J., Osterbart R., and Winters J. M. 1998. 76 mas speckle-masking interferometry of IRC +10 216 with the SAO 6m telescope: Evidence for a clumpy shell structure. *Astronomy and Astrophysics* 333:L51–L54.

Wopenka B. and Pasteris J. D. 1993. Structural characterization of kerogens to granulite-facies graphite: Applicability of Raman microprobe spectroscopy. *American Mineralogist* 78:533–557.

Zinner E., Amari S., Wopenka B., and Lewis R. S. 1995. Interstellar graphite in meteorites: Isotopic compositions and structural properties of single graphite grains from Murchison. *Meteoritics* 30:209–226.

Zinner E., Nittler L. R., Gallino R., Karakas A. I., Lugaro M., Straniero O., and Lattanzio J. C. 2006: Silicon and carbon isotopic ratios in AGB stars: SiC grain data, models, and the Galactic evolution of the Si isotopes. *The Astrophysical Journal* 650:350–373.